Timing and mechanisms of sediment accumulation and pedogenesis: Insights from the Po Plain (northern Italy)

**Abstract**

Paleosol stratigraphy in the Po Plain, reconstructed through sedimentological analysis and correlation of ca. 170 core data chronologically constrained by 376 radiocarbon dates, revealed strict relationships between pedogenetic and fluvial processes in alluvial and paralic environments. Vertically stacked, weakly developed paleosols within Upper Pleistocene and Holocene mud-prone strata testify to intermittent pedogenesis, periodically interrupted by overbank sedimentation. Individual paleosols are laterally traceable for tens of km and exhibit A-Bk-Bw, A-Bk or A-Bw profiles. Stratigraphically ordered $^{14}C$ calibrated ages from A horizons testify to slow aggradation during 4-6 thousand years-long exposure periods. Burial ages, with an error of few centuries, are provided by plant debris at the top of A horizons.

Millennial-scale climate oscillations and glacio-eustasy are the main drivers of the pedo-sedimentary evolution of the area during the last 50 kyr. Pleistocene (P) paleosols developed in well-drained floodplain environments, dissected by fluvial incision, during relatively warm periods. Overbank sedimentation and paleosol burial occurred during colder phases. High-sediment-supply during the Last Glacial Maximum hindered pedogenesis and led to the accumulation of 3-10 m-thick overbank strata. Widespread soil development (paleosol PH) occurred at the end of Last Glacial Maximum, following glaciers retreat and afforestation of drainage basins. At distal locations, paleosol PH was progressively buried under estuarine sediments during the Holocene phases of post-glacial sea-level rise. Beyond the area of marine influence, burial ages of paleosol PH change from a place to another without specific spatial trends and reflect upstream fluvial sedimentation dominated by avulsions and deposition of spatially restricted alluvial units. Holocene (H) paleosols show a poor correlation potential and laterally variable degree of maturity that reflect avulsive

sedimentation patterns and crevassing. Deforestation and land reclamation affected pedo-sedimentary processes during the last 6 kyr.

**Keywords**

Paleosol stratigraphy, pedo-sedimentary evolution, radiocarbon dates, climate change, eustasy, Late Quaternary

## 1. INTRO

In alluvial settings, the development and burial of soil horizons are intimately related to fluvial activity (Kraus and Bown, 1993) and governed by a variety of factors. High sediment supply and fluvial aggradation inhibit pedogenesis (Demko et al., 2004), whereas low sediment supply and fluvial incision promote soil development in interfluvial areas (Blum and Törnqvist, 2000). Climate influences the amount of sediment delivered to the basins, modulating the magnitude and type of precipitations, the vegetation cover of drainage areas and the river's transport capacity (Vandenberghe, 2003). Alluvial sedimentation can be locally hindered or enhanced by tectonic movements (Holbrook and Schumm, 1999; Viseras et al., 2003; Benvenuti et al., 2008; Pati et al., 2019), differential subsidence (Cohen et al., 2003) or by avulsions and other processes related to the intrinsic dynamics of the fluvial apparatus (Kraus, 1999; Cleveland et al., 2007; Hajek and Wolinsky, 2012). In coastal settings, fluvial dynamics are strongly influenced by sea-level oscillations (Atchley et al., 2004; Blum et al., 2013). Incised valleys (and associated interfluve paleosols) related

to glacio-eustasy are a widely recognized trait in the sedimentary record (Shanley and McCabe, 1994; Aitken and Flint, 1996; McCarthy and Plint, 1998; Plint et al., 2001; Gibling et al., 2011).

The causal relationships between paleosol formation and alluvial sedimentation have been reconstructed in ancient alluvial successions, where the geometric relationships between paleosols and associated fluvial sediment bodies are superbly exposed (Gibling and Bird, 1994; McCarthy and Plint, 2003; Dubiel and Hasiotis, 2011; Soares et al., 2020). However, the role of distinct controlling factors on paleosol development and burial can hardly be assessed (Wright and Marriott, 1993; Atchley et al., 2004), because of the temporal resolution of pre-Quaternary dating methods, insufficient to describe pedo-sedimentary processes which typically act at millennial time scales (Rasbury et al., 1997; Hofmann et al., 2017). Furthermore, diagenesis may have substantially modified soil properties after burial, hindering comparison with modern soils and the reconstruction of the soil-forming environment (Trendell et al., 2012).

Improved techniques of subsurface investigation have recently prompted the study of buried upper Quaternary alluvial successions (Choi, 2005; Tsatskin et al., 2015; Amorosi et al., 2017a,b). In this relatively narrow time window, drainage areas, ecosystems and soil-forming environment did not change significantly. Moreover, the high temporal resolution of Quaternary dating methods permits to link unequivocally pedogenetic processes to a well-known climate and eustatic history.

Radiocarbon is probably the most reliable dating method for the last 50 kyr (Reimer et al., 2020). However, numerous uncertainties remain in the interpretation of $^{14}C$ dates from paleosols. Organic carbon is continuously incorporated in soils, and subjected to complex, and not totally understood, biological and physical transformations (Larionova et al., 2017; Meingast et al., 2020). These processes can act at different velocity and magnitude, depending on climate, morphology of the exposed surface, parent material, and vegetation (Alexandrovskiy and Chichagova, 1998; Kleber, 2010).

This study is based on refined pedostratigraphic reconstructions and on a vast $^{14}C$ dataset which permitted to chronologically constrain the major architectural and facies changes. The primary aim of this research is to understand the causes and mechanisms of soil development and burial in an alluvial-deltaic setting and its relation to fluvial and coastal dynamics. To this purpose, we focused on Upper Pleistocene-Holocene paleosols and on their stratigraphic relationship with older, coeval and younger pedo-sedimentary units. Secondary objectives are to discuss: (i) the relative role of global and local controlling factors on soil development and burial; (ii) the potential use (and major limitations) of radiocarbon to assess the exposure age of paleosols.

## 2. GEOLOGICAL SETTING

### 2.1. Structural setting and basin-scale stratigraphy

The Po sedimentary basin is enclosed in a natural amphitheatre bordered by the Alps, to west and to the north, and by the Apennines, to the south. The eastward prolongation of the Po Plain is the Adriatic epicontinental sea (Fig. 1). The most external thrusts of the Southern Alps and of Apennines, showing opposite vergence, locally face each other beneath the Po Plain (Fantoni et al., 2004). South-Alpine buried thrusts are arranged in a single wide arc running from Milan to the Garda Lake (Vannoli et al., 2015). The Apennine front is composed of three tectonically active arcuate thrust systems: from west to east, the Monferrato, Emilia and Ferrara-Romagna Arcs (Ghielmi et al., 2013). Thrusts of the Emilia and Ferrara Arcs are sealed beneath a pile of sediments with extremely variable thicknesses (from a few hundred metres to ca. 8 km; Amadori et al., 2019). These lateral variations in thickness are controlled by lateral changes in subsidence rates (Campo et al., 2020),

120 ranging between zero and 2 mm/y (Bruno et al., 2020a). The northern margin of the Apennines,
121 which corresponds to an out-of-sequence system of N-NE verging thrusts (Maestrelli et al., 2018),
122 has been involved in a generalized uplift since the Early Pleistocene (Argnani et al., 2003).
123 The Po Basin fill shows and overall regressive trend from deep-marine to continental and coastal
124 units (Ghielmi et al., 2013). Widespread alluvial sedimentation started in the Po Plain around 870
125 kyr B.P. (Muttoni et al., 2003, 2011; Gunderson et al., 2014). The Po River, flowing in W-E direction,
126 divides the alluvial plain in two sectors (Fig. 1A). In the norther sector, Alpine tributaries flow
127 entrenched in Pleistocene sandy units (Ravazzi et al., 2012; Fontana et al., 2014; Bruno et al., 2018).
128 To the south, paleosol-bearing Pleistocene muds are sealed by a thick (up to 30 m) Holocene alluvial
129 and paralic succession (Amorosi et al., 2017a, b). Early Holocene estuarine deposits typically onlap
130 onto Upper Pleistocene alluvial strata, testifying to the progressive drowning of the alluvial plain
131 after 11.5 cal kyr B.P. (Bruno et al., 2017). Following stabilization of sea-level, the Middle-Late
132 Holocene records the progressive filling of the Po estuary and the successive delta progradation
133 (Amorosi et al., 2017b, 2019).
134
135 **2.2. Paleosols of the Po Basin**
136
137 Highly weathered rubified soils have been reported from the Po Basin margin (Cremaschi, 1987;
138 Garzanti et al., 2011) and from isolated hills in the alluvial plain, generated by South-Alpine (Zerboni
139 et al., 2015) and Apennine blind thrusts (Zuffetti et al., 2018). In depocentral areas, mature paleosols
140 are replaced by sequences of aggradationally stacked, weakly developed paleosols laterally
141 traceable for tens of km (Amorosi et al., 2017a). A series of closely spaced paleosols, marking the
142 MIS 3/MIS 2 transition, has been described as the equivalent of the Interfluve Sequence Boundary
143 (McCarty and Plint, 2003) in a high accommodation setting, due to its peculiar geometric

144 relationships with genetically related fluvial-channel bodies (Amorosi et al., 2017a). The most
145 widespread paleosol reported in the Po Plain marks the Pleistocene-Holocene boundary and
146 responds to several local names: 'Caranto' in the Venetian Plain (Mozzi et al., 2003), 'Ringhiera
147 paleosol' in the Romagna area (Ravazzi et al., 2006), 'YD paleosol' in the Po Delta Plain (Amorosi et
148 al., 2017b; Morelli et al., 2017), 'PH paleosol' in the Bologna urban area (Amorosi et al., 2014; Bruno
149 et al., 2020b; this name will be used in this paper). Although a wide literature reported the existence
150 of this pedogenized horizon, the mechanisms and causes of its formation and burial are not yet fully
151 understood. More discontinuous paleosols have been described from the Holocene succession
152 (Bruno et al., 2015, 2013).
153
154
155 **3. METHODS**
156
157 This work is based on the sedimentological and stratigraphic analysis of core material. Sixty-nine
158 cores, 30-50 m deep (red circles in Fig. 2), were analysed and sampled for radiocarbon dating. For
159 each core lithology, grainsize, colour and accessory materials (vegetal and shell macrofossils,
160 carbonate concretions, redoximorphic features) were reported. The reaction to HCl was tested as a
161 qualitative indicator of the presence of calcium carbonate. Resistance was measured on fine-grained
162 sediments with a Pocket Penetrometer (PP). One hundred and seventy-two wood, peat, vegetal-
163 remains and bulk-soil samples were dated at the KIGAM AMS laboratory (Daejeon, Republic of
164 Korea) and at the Ion Beam Physics laboratory of the ETH (Zurich, Switzerland, Synal et al., 2007).
165 Samples were collected fresh from the innermost part of the core and desiccated in a 40° oven. The
166 humin fraction was separated through acid-alkali-acid (AAA) pre-treatment and AMS dated. Humic

167 acids, extracted from 9 bulk soil samples were also dated. Conventional $^{14}C$ ages were calibrated
168 using OxCal 4.4, with the IntCal 20 curve (Reimer et al., 2020).
169 More than 100 core descriptions from previous works and from the database of the Geological,
170 Seismic and Soil survey of Regione Emilia-Romagna (yellow circles in Fig. 2) were reinterpreted
171 following calibration with new cores. These descriptions provide information on lithology, colour,
172 consistency, reaction to 10% HCl, pocket penetrometer measurement and radiocarbon dates.
173 Additional 204 radiocarbon dates derive from previously published works (Geological Map of Italy
174 to scale 1:50.000; Ravazzi et. al., 2006; Cacciari et al., 2017; Marabini and Vai, 2020).
175
176
177 **4. RESULTS**
178
179 **4.1. Sedimentary facies**
180
181 The sedimentological analysis of the studied cores led to the identification of several facies
182 associations which belong to alluvial, deltaic, estuarine and shallow-marine depositional
183 environments. To the purposes of this paper, we will describe in detail four main facies associations,
184 which are part of the alluvial, upper delta-plain and inner estuary depositional systems. For other
185 facies associations, the reader is referred to Amorosi et al. (2017b, 2019) and Bruno et al. (2017).
186
187 4.1.1. Fluvial channel-related facies association (FCR)
188
189 This facies association is composed of cross-stratified or laminated coarse-to-fine sand with local
190 mud intercalations (Fig. 3). The occasional presence of floated woods or plant debris is recorded.

191 Marine or lagoonal macrofossils are absents, whereas shell fragments of freshwater gasteropods
192 are seldom encountered.
193 Based on lithology, sedimentary structures and on the lack of marine and lagoonal macrofossil,
194 these coarse-grained deposits are interpreted as related to fluvial activity (in-channel deposition,
195 bar migration, crevassing, proximal overbank; Miall, 1985; Toonen et al., 2012; Aslan, 2013).
196
197 4.1.2. Freshwater swamp and marsh (SM)
198
199 This facies association is dominated by fine-grained material, with abundant wood, vegetal
200 remains and peat (Fig. 3). Peat horizons, 5-30 cm thick, are composed of poorly decomposed woody
201 material and are separated by grey (2.5 YR 7.1, 7.5 YR 8/1), peat-free clays. Freshwater fossils were
202 locally encountered. Consistency is very weak and PP values are < 1 kg/cm$^2$. Carbonate concretions
203 and redoximorphic features are absent. This facies association shows poor lateral extent in the
204 Upper Pleistocene succession. On the contrary, in Holocene distal deposits it is volumetrically
205 dominant and only locally interrupted by channel-related sands.
206 The grainsize of this facies group denotes a low-energy depositional environment. The
207 abundance of poorly decomposed organic material and the lack of oxidation suggest the setting of
208 reducing conditions in submerged environments. The latter were likely isolated ponds during the
209 Late Pleistocene, and swamp-marshes part of wider delta-plain and bayhead delta systems during
210 the Holocene (Amorosi et al., 2017b; Bruno et al., 2017; Cacciari et al., 2020). Peat horizons
211 separated by peat-free clays testify to intermittent sedimentation, with peat accumulation during
212 sedimentation breaks (Hijma and Cohen, 2011; Ishii et al., 2016; Bruno et al., 2019).
213
214 4.1.3. Poorly drained floodplain (PDFP)

This facies association is composed of grey (7.5 YR 6/1) silty clays with faint lamination given by millimetre-scale silt intercalations. Soft and isolated carbonate concretions (CC in Fig. 4) and sparse plant debris (UOM in Fig. 4) were seldom encountered. Redoximorphic features are lacking. Freshwater gasteropods were seldom encountered. Consistency is weak to firm. Pocket penetrometer values are in the range of 1-2 kg/cm$^2$.

Based on grainsize and fossil content, this facies association is interpreted as deposited in a distal fluvial environment, occasionally subjected to river flooding. Lack of redoximorphic features suggests a groundwater table fluctuating close to the topographic surface (poorly drained floodplain). The amount, distribution and type of secondary calcite are consistent with this interpretation.

#### 4.1.4. Well-drained floodplain (WDFP)

This facies association is composed of firm-to-hard clayey silts and silty clays. Sedimentary structures are absent. By contrast, polygonal structures, desiccation cracks and rootlets are commonly observed. A well-expressed horizonation is given by colour and $CaCO_3$ distribution (Fig. 3). Dark horizons, showing weak or no reaction to HCl alternate with lighter horizons showing strong reaction to HCl. Carbonate concretions, in the form of coalescent nodules, coatings, filaments and sub-horizontal bands are observed in lighter horizons. Redoximorphic features, in the form of orange mottles or bands (RF in Fig. 6), are commonly observed at the mesoscale. Plant debris and freshwater gasteropods are seldom encountered. PP values are > 2 kg/cm$^2$.

As for facies PDFP, grainsize and fossil content point to a distal fluvial environment, occasionally inundated by river waters (Collinson, 1996). The alternation of dark and light horizons is interpreted

as the result of multiple phases of soil development interrupted by overbank deposition and paleosol burial. Dark colour reflects the accumulation and decomposition of organic matter in the topsoil (Bruno et al., 2020b). Carbonate distribution, with carbonate-free horizons overlying $CaCO_3$ enriched horizons, is interpreted as the result of carbonate leaching from the topsoil (A horizon) and illuviation to the underlying Bk horizon (Boul et al., 2011). Carbonate mobilization requires the percolation of meteoric waters in a vadose zone. We, thus, argue that the groundwater was located a few metres below the topographic surface during subaerial exposure (well-drained floodplain).

### 4.2. Paleosol stratigraphy

Paleosols were identified at three stratigraphic intervals in the Upper Pleistocene-Holocene succession of the Po Plain.

The lower interval is composed of a series of closely-spaced paleosols (paleosols P in Figs. 4, 5 and 6), whose cumulative thickness is in general < 5 m. Calibrated ages span from the $^{14}C$ detection limit (~50 kyr B.P.) to ~23 kyr B.P. (Figs. 5 and 6). These paleosols show A-Bk-Bw or A-Bk profiles. A horizons, 30-50 cm thick, are decalcified (Bruno et al., 2020b; Amorosi et al., this volume) and present diffuse organic matter (DOM in Fig. 4) and slight bands of Fe oxides and/or hydroxides (Fig. 3). Undecomposed organic matter was not observed and carbonate concretions have locally been reported from the base and the top of these horizons. Bk horizons are typified by high $CaCO_3$ content (30-40% of the total volume, Bruno et al., 2020b). Carbonate concretions are abundant as coalescent nodules or whitish sub-horizontal bands (evolutionary stage II of Gile et al., 1981; Machette, 1985). Transition to overlying and underlying horizons is in general gradational. Bw horizons show moderate $CaCO_3$ content (Bruno et al., 2020b; Amorosi et al., this volume) and faint

mottles of Fe oxides and-or hydroxides. Evidences of clays mobilization (Bt horizons) were not observed. At distal locations, these paleosols may show less clear horizonation (A-Bw profile) or may be replaced by coeval peat-bearing swamp deposits (Fig. 5).

In the second interval, a single paleosol (paleosol PH, Figs. 4, 5 and 6) is encountered at the top of a 3-10 m thick sedimentary unit composed of overbank muds and subordinated channel-related sands (Last Glacial Maximum Sedimentary Unit, LGM SU in Figs. 4, 5 and 6). Textural characters of paleosol PH vary from proximal to distal locations. At inland locations (core EM15, Fig. 3), paleosol PH shares many characteristics with older P paleosols: (i) a carbonate-free, brown (10YR 4/4, 3/3) A horizon, up to 100 cm thick, with DOM and RF; (ii) a lighter Bk horizon with abundant nodules or bands of secondary calcite (evolutionary stage II); (iii) a Bw horizon showing evidence of incipient alteration. At more distal locations (cores EM1 and EM3, Fig. 3), paleosol PH exhibit a grey (5Y 4/1, 2.5Y 6/1) decalcified A horizon, 30-50 cm thick, with DOM. Plant debris, absent in the lower part, become increasingly abundant upsection and, at places, grade into the overlying peats (see core B3, Fig. 4). The underlying Bk horizon, when present, is relatively thin (a few dm), with secondary calcite in the form of nodules, coatings or filaments (evolutionary stages I and II). Redoximorphic features were not observed at the mesoscale along the whole soil profile.

In the third interval, dated to the Holocene, paleosols (H1 and H2 in Figs. 4, 5 and 6) have been observed only at inland locations. At distal locations, they are replaced by coeval estuarine and deltaic deposits. H paleosols have poor correlation potential and their textural features vary dramatically from a place to another, without specific spatial trends. In few localities, they show characteristics similar to those of their Pleistocene counterparts. At places, they are barely identifiable due to a poorly developed horizonation. Archeological artifacts are increasingly abundant in younger paleosols.

Paleosols P and PH bound nearly tabular sediment packages and are locally replaced by coeval incisions filled with FCR or SM deposits (see cores CNT, RN3 and EM2, Fig. 5). On the contrary, Holocene paleosols overlie or are overlain by CR facies (see cores MW and 15, Figs. 5 and 6). Alluvial units delimited by these soil horizons are poorly extended and typically wedge out laterally or downdip (Figs. 5 and 6).

### 4.3. Radiocarbon dating of paleosols

Upper Quaternary successions provide the great opportunity to link pedo-sedimentary events to the detailed climatic and eustatic history described in a vast literature (eg. Clark and Huybers, 2009; Lambeck et al., 2011; Rasmussen et al., 2014). Assessing the timing of soil development and burial is crucial to disentangle the relative influence of global and local factors. This chapter summarizes observations deriving from the analysis of a chronological database composed of 376 radiocarbon dates (160 from paleosols).

Along single cores, multiple dating of A horizons yielded stratigraphically ordered ages, spanning 3-5 kyr (see cores B3, RW28 and 13, Figs. 4, 5C and 6). Only in core SPR (Fig. 5C) two samples from the base and the top of the same A horizon provided similar ages. In distal cores, plant debris from topmost A horizons yielded ages that are considerably younger (up to 5 kyr) than those from bulk-soil samples and just a few centuries older than those from overlying SM peats (see cores EM1, EM3 and B3, Figs. 3, 4 and 5). Dates from A horizons indicate aggradation at extremely low rates (0,05-0,23 mm yr-1) during soil development. Accumulation rates above or between paleosols are at least one order of magnitude grater (> 1 mm/yr). Distinct ages were also obtained from different

309 fractions extracted from the same sample. Particularly, humic acids yielded, in 9 cases out of 10,
310 ages older than those obtained from the humin fraction (Table 1).

311 Dates from bulk-soil samples change also laterally, along the same paleosol, spanning in a range
312 of 4-6 kyr (Fig. 3). No specific trend was observed from proximal to distal locations. Ages also change
313 over short distances, as observed in the Bologna area. In the Two Tower Medieval district, where
314 distance between cores is just 10-20 m, six samples from paleosol P3 yielded ages in the range of 3-
315 4 kyr (Fig. 6).

316 The frequency distribution of radiocarbon dates from paleosols (grey rectangles in Fig. 7) shows
317 a major peak between 14 and 10 kyr B.P., related to the PH paleosol. Samples from the P paleosols
318 yielded ages clustered around three minor peaks (P1, P2 and P3, Fig. 7), at 46-41, 38-32 and 29-25
319 cal kyr B.P., respectively. The overall decay with time in the number of $^{14}C$ dates across the
320 Pleistocene simply reflects the fact that older sediments were penetrated by a progressively lower
321 number of cores. A decline in the number of $^{14}C$ dates from soil samples is also recorded towards
322 younger ages, together with a sharp increase in dates from SM and PDFP deposits. Ages from
323 Holocene soil samples are clustered around two peaks. The older peak reflects, in part, the youngest
324 ages from paleosol PH and in part dates from a distinct paleosol (H1 in Figs 4, 5 and 6) observed at
325 several inland locations. In the Bubano Quarry (BQ in Fig. 5C), 5 m-thick overbank strata separate
326 H1 from PH. In the Bologna area (core 16, Figs. 4 and 6), paleosol H1 bears Neolithic and Eneolithic
327 artefacts (Bruno et al., 2013). The second peak (H2, Fig. 7) corresponds to another archeological
328 level, rich in Late Bronze Age, Iron-Age and Roman rests (IR paleosol of Bruno et al., 2013), which
329 was buried in large part of the Po Plain during the Middle Ages (see core CRV, Fig. 5A). Locally, this
330 paleosol is still exposed (Fig. 5). Interestingly, the maximum number of $^{14}C$ dates from facies FCR is
331 recorded between H2 and H1.

332

## 5. DISCUSSION

### 5.1 Use and limitations of radiocarbon for the estimation of the exposure age of paleosols

The use and reliability of radiocarbon dates from paleosols have been widely debated because, unlike plant macrofossils, which preserve the particular $^{14}C$ content of the moment of grow, soils are open systems where organic carbon is continuously incorporated, humified and-or oxidized to $CO_2$ before burial (Orlova and Panychev, 1993; Martin and Johnson, 1995; Gaudinski et al., 2000). Therefore, $^{14}C$ ages from paleosols reflect the mean residence time of the organic carbon plus the time of burial (Matthews, 1980; Geyh et al., 1983). The amount of organic carbon added to a soil and the velocity of its transformation processes change from place to place as a function of climate, vegetation and parent material (Reimer et al., 2020). Moreover, turnover and breakdown of organic matter may lead to the redistribution of $^{14}C$ ratios in different soil fractions. As a result, apparently conflicting ages can be obtained from the same paleosol (Figs. 5 and 6) and from different soil fractions (Table 1). Because of this inherent variability, many authors concluded that radiocarbon dates from soils are unreliable and the concept of "age" cannot be strictly applied to paleosols (Gilet-Blein et al., 1980; Becker-Heidmann et al., 2002). However, if not subjected to post-burial contamination (e.g. rootlets), paleosols should yield ages scattered within its formation period. The estimation of the length of this period, which can attain several millennia, is an intriguing goal for Quaternary paleosol stratigraphers.

The lack of evidence of clay mobilization, the evolutionary stage of secondary calcite and the limited rubefaction suggest that Po Plain paleosols evolved over relatively short periods. Radiocarbon ages from deposits below and above paleosols constrain their exposure period within

10-12 thousand years (Figs. 5 and 6). Dates from paleosols are within the narrower range of 4-6 millennia and provide a robust constrain for stratigraphic correlations over long distances (Amorosi et al., 2017a). More complex is the precise assessment of the ages that mark the onset and end of pedogenesis for each paleosol, even if radiocarbon dates are available from the base and top of A horizons. Previous work has demonstrated that, although some organic carbon can remain in soils for millennia (Feng, 2009), the oldest organic fraction accumulated at the onset of pedogenesis may have been completely replaced by younger organic carbon (Scharpenseel, 1971; Alexandrovskiy and Chichagova, 1998) introduced by roots in the deepest soil horizons. Thereby, radiocarbon dates from organic-sediment samples collected from the base of the A horizon may not be representative of the onset of soil formation (Gilet-Blein et al., 1980; Alexandrovskiy and Chichagova, 1998). Several factors influence carbon turnover times in soils (Kleber, 2010; Chen et al., 2013; Pandey et al., 2014). Particularly, carbon renewal is slower in colder climates and in deep soil horizons (Alexandrovskiy and Chichagova, 1998; Gaudinski et al., 2000; Fontaine et al., 2007). Therefore, for soils that developed in cold climatic conditions, such as paleosols P3, which formed at the onset of Last Glacial Maximum, dates from the base of the A horizon should better approximate the onset of pedogenesis. This assumption is corroborated by dates from core B3 (Figs. 3, 4 and 5), where the oldest age from paleosols P3 partially overlaps the age from underlying paleosol P2. For paleosols developed in warmer periods (PH and H paleosols), ages from the base of A horizons may post-date the onset of pedogenesis.

Sediment samples collected from the top of A horizons may be older than burial time, because a certain amount of time is required for litter humification and mineralization (Chichagova and Cherkinsky, 1993). At inland locations of our study area, where O horizons are generally not preserved, burial ages cannot be assessed precisely. Available dates permit to assert, for example, that paleosol PH was buried after 10.3 kyr B.P. in core 13 (Figs. 4 and 6) and between 14.3 and 8.6

kyr B.P. in core 201S4 (Fig. 5). Conversely, at distal locations, plant macrofossils preserved in the topsoil provides ages that approximate the paleosol burial age with an error of a few centuries. For example, in EM1, where estuarine sedimentation was already established around 8.1 kyr B.P., burial of paleosol PH occurred around 8.5 kyr B.P. (Figs. 3, 4 and 5).

Age/depth gradients, like those observed in the Po Plain paleosols, have been reported from several soil profiles (Matthews, 1981; Matthews and Dresser, 1983; Alexandrovskiy and Chichagova, 1998; Becker-Heidmann et al., 2002) and can possibly be explained by the fact that the amount of carbon added to the topsoil through litter accumulation is in general order of magnitudes greater than the one introduced in deeper soil horizons via roots exudation (Fontaine et al., 2007). The measured accumulation rates, incompatible with alluvial sedimentation, suggest that litter accumulation accounted for soil aggradation during exposure, with a possible contribution of wind-transported dust. Therefore, paleosols from the Po Plain represent condensation horizons, rather than depositional hiatuses. On the contrary, sedimentation between pedogenetic phases seems a quasi-instantaneous process (see ages from P2 and P3 in core B3, Figs 4 and 5). Paleosols aggradation is also testified by the presence of carbonate concretions in lower A horizons, likely related to the upward migration of the eluvial-illuvial (A-B) boundary, and by vertically stacked sub-horizontal bands of secondary calcite in Bk horizons (Fig. 3). Carbonate concretions in upper A horizons, on the other hand, reflect post-burial illuviation from overlying paleosols. For this reason, we avoided radiocarbon dating of carbonates and removed secondary calcite in acid steps of the AAA sample preparation, before AMS analysis. Humic acids are also considered as a mobile compound, which may yield anomalously young ages due to contamination from overlying strata (Matthews, 1980). In our case, the oldest ages are provided by humic acids (Table 1). We thus excluded contamination from overlying strata during each phase of pedogenesis.

405

406 **5.2. Pedo-sedimentary evolution of the Po Plain and controlling factors**

407

408 With the chronological constraint of 376 radiocarbon dates, the alluvial succession of the
409 southern Po Plain provides an unprecedent record of pedo-sedimentary events across the last 50
410 kyr.

411 Aggradationally stacked paleosols 'P' developed during the Late Pleistocene, when the Adriatic
412 coastline migrated in response to the stepwise sea-level fall toward its lowstand position, ~300 km
413 away from the modern one (Pellegrini et al., 2018). Among P paleosols, only P3 developed during a
414 phase of sea-level drop (~30–50m between 30 and 24 cal ka BP, Peltier and Fairbanks, 2006; Fig.
415 7B). Conversely, P1 and P2 developed in a period characterized by low-amplitude sea-level
416 oscillations (Chappell, 2002; Fig. 7B). Far from the influence of sea-level change, pedo-alluvial
417 processes are controlled by the balance between sediment supply and water discharge (Blum and
418 Törnqvist, 2000). Low sediment supply-discharge ratios result in channel incision and soil
419 development in the adjacent interfluves, whereas high sediment supply-discharge ratios promote
420 fluvial aggradation and paleosol burial (Demko et al., 2004). Bruno et al. (2020b) documented that
421 soil development and burial during the Late Pleistocene was mainly controlled by changes in
422 vegetation driven by climatic oscillations at the scale of Bond cycles (Bond et al., 1993). Soils started
423 to form at the onset of Bond cycles, when warm climate conditions favoured the spread of dense
424 forests (Magri, 1999; Fletcher et al., 2010), which protected the Apennine drainage basins from
425 erosion (low sediment supply). Soil development was systematically interrupted during the
426 subsequent cold phases, at the culmination of Bond cycles, corresponding to North Atlantic Heinrich
427 events (light blue vertical lines in Fig. 7B). These periods record generalized forest retreats (Fletcher
428 et al., 2010; Helmens, 2014), which enhanced erosion in the drainage basins and sediment transfer
429 to the alluvial plains. Increased sediment supply promoted the filling of fluvial incisions and the

burial of formerly exposed interfluves by overbank sedimentation. Thin sediment packages were deposited between two successive phases of subaerial exposure (Figs. 3 to 6). These deposits (and, partly, the underlying paleosols) were modified during the successive pedogenetic phase. A similar response to millennial-scale climate oscillations has been observed in loess paleosol-bearing successions (Rousseau et al., 2011, 2007; Moine et al., 2017; Zeeden et al., 2018).

The Last Glacial Maximum was characterized by deposition of thick and widespread fluvial-channel gravel-sand bodies in the Po Plain (Ravazzi et al., 2012; Campo et al., 2016) and in other alluvial systems worldwide (Lewis et al., 2001; Briant et al., 2005). Alpine glaciers, which extended down to the Po Plain margin, supplied huge amounts of sediments to the related fluvio-glacial systems (Fontana et al. 2014). In the Apennine domain, high sediment supply, favoured by a predominantly herbaceous vegetation cover of drainage basins (Vescovi et al., 2010), resulted in the deposition of the LGM SU, which bears poor evidence of pedogenesis (Figs. 4, 5 and 6).

Above the LGM SU, PH is the most widespread paleosol in the Po Plain. This surface yielded radiocarbon dates spanning between ~17 and 6 kyr B.P. (Fig. 8), but mostly clustered around 14 and 10 kyr B.P. (Fig.7). The precise assessment of the age of PH formation is hampered by paucity of dateable material from the underlying LGM SU. However, available dates indicate that the onset of post-LGM pedogenesis was diachronous across the Po Plain, without a specific spatial trend (Fig. 8). Whereas in the Bologna area PH started to develop at least 16.8 kyr B.P. (see core RW28, Figs 6 and 8), in the Romagna plain (Bubano Quarry - BQ, in Figs 5C and 8) pedogenesis started after 14.4 kyr B.P. (Ravazzi et al., 2006). We argue that post-LGM pedogenesis was favoured by decreased sediment supply related to the progressive afforestation of the area (Pini et al., 2010; Vescovi et al., 2010; Campo et al., 2020), with diachroneity possibly related to particular local conditions (e.g. distance from active channels). North of the Po River, in the Alpine tributary system, fluvial incision

occurred soon after glacial retreat (~17 kyr B.P., Monegato et al., 2017), due to sediment trapping in lakes which formed in place of abandoned glacial amphitheatres (Fontana et al., 2014).

Interestingly most of the $^{14}C$ dates from paleosol PH post-date the Oldest Dryas (OD in Fig. 7). The clustering of dates around the Younger Dryas in the Po delta plain (Figs. 7A and 8), suggested a possible control of this cold event on paleosol formation (Amorosi et al., 2017b, Morelli et al., 2017). The wider dataset shown in this work highlights that pedogenesis started in many sites of the Po Plain at least during the Bølling and Allerød warm phases (BA in Fig. 7A). Unlike cold phases at the culmination of pre-LGM Bond cycles, the Younger Dryas cold spell did not lead to paleosol burial. This event was probably too short-lived to promote the filling of fluvial incisions and overbank sedimentation. Paleosol development recorded after LGM in other alluvial (Mol, 1997; Choi, 2005; van Balen et al., 2010; Janssens et al., 2012) and eolian (Kaiser et al., 2009; Hošek et al., 2017) successions, indicates a likely climate control at a supra-regional spatial scale. Progressively warmer conditions lead to widespread afforestation and reduced sediment supply (Fletcher et al., 2010; Helmens, 2014).

Whereas Alpine rivers still flow entrenched in Pleistocene deposits, Apennine incisions were filled during the Early Holocene (see cores RN3 and EM2, Fig. 3C) and paleosol PH was buried soon after. In the coastal plain, where paleosol PH is encountered at greater depths beneath estuarine deposits, burial ages show an overall inverse power law with elevation (Fig. 9) that reflects the progressive drowning of the area during the early Holocene sea-level rise (Bruno et al., 2017). Slight dispersion of data may reflect post-burial deformation of paleosol PH by differential subsidence and neotectonics (Amorosi et al., 2021). In the area under marine influence (shades of blue in Fig. 10), burial ages decrease landwards from ~11.5 to 5.4 kyr B.P.. This overall spatial trend is not recorded in two isolated areas, where paleosol PH and older paleosols are upbended (see also Fig. 5C). In cross-sections, the progressive drowning of paleosol PH is testified by onlap terminations of

Holocene flooding surfaces (Fig. 5A). These horizons, associated to prominent facies backstepping, are coeval to the main Holocene melt water pulses (MWP-1b, 1c, 1d; Fig. 7B), which forced the landward migration of the Po estuary across the study area. The effects of MWP-1A are not recorded in the study area, which was too far from the coastline at that time (Storms et al., 2008).

Pedo-sedimentary features of paleosol PH reflect this evolutionary history. Carbonate redistribution along the soil profile and relatively low amounts of organic carbon in the A horizons (Amorosi et al., this volume) are indicative of a low groundwater table (Kalisz et al., 2010), enhanced by fluvial incision during the early phases of soil development (Tebbens et al., 1999). Preserved plant debris in the topsoil, radiocarbon dated to the early Holocene (Figs. 4 and 5), reflects the progressive rise in groundwater table (Bohacs and Suter, 1997) up to the setting of waterlogged conditions and to the accumulation of peat beds (Diessel, 1992; Richardson and Vepraskas, 2001; Stolt and Rabenhorst, 2011). The rise of the groundwater table, forced by sea-level rise (Kosters and Suter, 1993; Törnqvist, 1993; Wadsworth et al., 2003), led to the progressive filling of Apennine fluvial incisions by fine-grained and organic-matter-rich estuarine strata (facies SM, cores RN3 and EM2 in Fig. 5C). The lack of fluvial sands (facies FCR) at the base of fluvial incisions, suggests that valley filling was promoted by eustasy rather than by an upstream increase in sediment supply (Kvale and Archer, 2007).

Beyond the area of marine influence, at elevations > -3 m, the burial age of paleosol PH is substantially unpredictable (Figs. 9 and 10). The dispersion of burial dates in this upstream sector reflects the dynamics of Holocene sedimentation, dominated by avulsion processes and by the deposition of poorly extended alluvial units (Figs. 5 and 6). This aspect is particularly evident in the Bologna area (Fig. 6): in core 16, for example, paleosol PH was already buried around 8.2 kyr B.P., when paleosol H1 was still developing (see also Fig. 4); in the nearby core 15, at a distance of just 224 m, the burial of paleosol PH occurred only around 7 kyr B.P.. The transition to an avulsive

sedimentation pattern at the onset of the Holocene, recorded in several worldwide fluvial systems (Phillips, 2011; Stouthamer et al., 2011), is an indirect consequence of the landward migration of the coastline, which dramatically reduced the area available for sediment storing and lowered rivers longitudinal gradients. Decreased stream power, and capability to erode banks and create space for sediment storage, led to river aggradation, crevassing and avulsions (Blum et al., 2013).

The discontinuity of Holocene paleosols (Figs. 5 and 6) reflects the limited areal extent of the sedimentary units on which they developed. Avulsive sedimentation patterns and crevassing also determined laterally variable maturity of Holocene paleosols. Indeed, soil development was interrupted only in restricted areas affected by alluvial deposition. In sediment-starved areas, soils continued to evolve. Lateral changes in soil maturity are observable in modern soils, which started to develop during the Late Bronze age (areas where H2 is still exposed – Fig. 5), and after the Middle Ages (areas where H2 is buried - Fig. 5).

The peak in radiocarbon dates from fluvial channel-related deposits, centred around 5-6 kyr B.P. (Fig. 7), corresponds to a generalized re-organization of the river network at the onset of Neoglaciation (Piovan et al., 2012; Bruno et al., 2015; Amorosi et al., 2017b), which led to the burial of paleosol H1. Slope instability and enhanced sediment production, recorded in the Northern Apennines since 5.5 kyr B.P. (Soldati et al., 2006; Picotti and Pazzaglia, 2008), likely reflect widespread deforestation of the Apennine drainage basins during the early Eneolithic (Cremaschi and Nicosia, 2012). The progressive return to stable floodplain conditions was paralleled by improved techniques of land reclamation and management from the late Bronze age to late Antiquity (Bruno et al., 2013).

## 6. CONCLUSIONS

Based on the sedimentological analysis and correlation of more than 170 core data, with the chronological constraint of 376 radiocarbon dates, this study provided new data on: (i) the complex relationships between pedogenetic, fluvial and costal processes in alluvial and paralic environments; (ii) the relative influence of global (i.e. climate and eustasy) and local (e.g. river avulsions) factors on soil development and burial; (ii) the use and limitations of radiocarbon to assess the exposure age of paleosols.

In the Upper Pleistocene-Holocene mud-prone succession of the Po Basin, vertically stacked, weakly developed paleosols testify to intermittent pedogenesis, periodically interrupted by overbank sedimentation. Radiocarbon analyses permitted to define the duration of the main phases of pedogenesis and to compare them to climate and eustatic curves.

Radiocarbon dates from paleosols (bulk-soil and plant-debris samples) and from underlying and overlying sedimentary units indicate exposure periods encompassing 4-6 millennia. This estimate is consistent with pedological features (e.g. type of secondary calcite, lack of illuvial clay, limited rubefaction), which denote incipient pedogenesis. Stratigraphically ordered $^{14}C$ calibrated ages within A horizons revealed that Po Plain paleosols are condensation horizons, which experienced slow aggradation during exposure (0,05-0,23 mm/yr) due to accumulation of plant litter, with a likely contribution of wind-transported dust.

Millennial-scale climate oscillations and glacio-eustasy concurred in driving the pedo-sedimentary evolution of the Po Plain during the Late Pleistocene. In particular, during the MIS 3, pedogenetic events were mainly controlled by changes in vegetation driven by climatic oscillations at the scale of Bond cycles. Paleosols developed in well-drained floodplain environments, dissected by fluvial incision, during relatively warm periods. Overbank sedimentation and paleosol burial

548 occurred during colder phases. During the Last Glacial Maximum, high-sediment-supply hindered
549 pedogenesis and led to the accumulation of 3-10 m-thick overbank strata.

550 Widespread soil development (paleosol PH) occurred at the end of the Last Glacial Maximum,
551 following glaciers retreat and afforestation of drainage basins. Burial of paleosol PH was
552 diachronous as indicated by radiocarbon dates from vegetal remains preserved at the topsoil. At
553 distal locations, paleosol PH was progressively drowned and buried under estuarine sediments
554 during the Holocene phases of post-glacial sea-level rise. Beyond the area of marine influence, burial
555 ages of paleosol PH change from a place to another without specific spatial trends, reflecting
556 upstream fluvial sedimentation dominated by avulsions.

557 Holocene (H) paleosols, observed at inland locations, grade seaward into coeval estuarine and
558 deltaic deposits. These pedogenized horizons show a poor correlation potential and laterally
559 variable degree of maturity that reflect avulsive sedimentation patterns and widespread crevassing.
560 Human activities (e.g. deforestation and land reclamation) became an increasingly important factor
561 affecting pedo-sedimentary processes during the last 6 kyr.

562 This study highlights the potential for paleoenviromental reconstructions of upper Quaternary
563 sedimentary successions. The pedo-stratigraphic approach adopted here, relying upon a robust
564 chronological framework, permitted to assess the temporal and spatial scale of pedogenetic events
565 and to discern the relative contribution of distinct controlling factors that typically act
566 contemporaneously.

567

568

569 **Acknowledgments**

570 We thank Mantana Maurer and Lukas Wacker and the AMS team of LIP ETH Zurich for their
571 support with sample preparation and AMS analysis.

572

573

574 **REFERENCES**

575

576 Aitken, J.F., Flint, S.S., 1996. Variable expressions of interfluvial sequence boundaries in the
577 Breathitt Group (Pennsylvanian), eastern Kentucky, USA. Geol. Soc. London, Spec. Publ. 104,
578 193–206.
579 Alexandrovskiy, A.L., Chichagova, O.A., 1998. Age of humic substances in paleosols. Radiocarbon
580 40, 991–997.
581 Amadori, C., Toscani, G., Di Giulio, A., Maesano, F.E., D'Ambrogi, C., Ghielmi, M., Fantoni, R., 2019.
582 From cylindrical to non-cylindrical foreland basin: Pliocene–Pleistocene evolution of the Po
583 Plain–Northern Adriatic basin (Italy). Basin Res. 991–1015. https://doi.org/10.1111/bre.12369
584 Amorosi, A., Bruno, L., Rossi, V., Severi, P., Hajdas, I., 2014. Paleosol architecture of a late
585 Quaternary basin – margin sequence and its implications for high-resolution , non-marine
586 sequence stratigraphy. Glob. Planet. Change 112, 12–25.
587 https://doi.org/10.1016/j.gloplacha.2013.10.007
588 Amorosi, A., Bruno, L., Cleveland, D.M., Morelli, A., Hong, W., 2017a. Paleosols and associated
589 channel-belt sand bodies from a continuously subsiding late quaternary system (Po basin,
590 Italy): New insights into continental sequence stratigraphy. Bull. Geol. Soc. Am. 129, 449–463.
591 https://doi.org/10.1130/B31575.1
592 Amorosi, A., Bruno, L., Campo, B., Morelli, A., Rossi, V., Scarponi, D., Hong, W., Bohacs, K.M.,
593 Drexler, T.M., 2017b. Global sea-level control on local parasequence architecture from the
594 Holocene record of the Po Plain, Italy. Mar. Pet. Geol. 87, 99–111.
595 https://doi.org/10.1016/j.marpetgeo.2017.01.020

596 Amorosi, A., Barbieri, G., Bruno, L., Campo, B., Drexler, T.M., Hong, W., Rossi, V., Sammartino, I.,
597 Scarponi, D., Vaiani, S.C., 2019. Three-fold nature of coastal progradation during the
598 Holocene eustatic highstand, Po Plain, Italy–close correspondence of stratal character with
599 distribution patterns. Sedimentology 66, 3029–3052.
600 Amorosi, A., Bruno, L., Campo, B., Costagli, B., Hong, W., Picotti, V., Vaiani, S.C., 2021. Deformation
601 patterns of upper Quaternary strata and their relation to active tectonics, Po Basin, Italy.
602 Sedimentology 68, 402–424. https://doi.org/10.1111/sed.12784
603 Amorosi, A., Bruno, L., Campo, B., Di Martino, A., I. Sammartino. Patterns of geochemical variability
604 across weakly developed paleosol profiles and their role as regional stratigraphic markers (Late
605 Pleistocene, Po Plain). Submitted to this volume.
606 Argnani, A., Barbacini, G., Bernini, M., Camurri, F., Ghielmi, M., Papani, G., Rizzini, F., Rogledi, S.,
607 Torelli, L., 2003. Gravity tectonics driven by Quaternary uplift in the Northern Apennines:
608 Insights from the La Spezia-Reggio Emilia geo-transect. Quat. Int. 101–102, 13–26.
609 https://doi.org/10.1016/S1040-6182(02)00088-5
610 Aslan, A., 2013. Sediments. Encycl. Quat. Sci. Second Ed. 663–675. https://doi.org/10.1016/B978-
611 0-444-53643-3.00111-4
612 Atchley, S.C., Nordt, L.C., Dworkin, S.I., 2004. Eustatic control on alluvial sequence stratigraphy: A
613 possible example from the Cretaceous-Tertiary transition of the Tornillo Basin, Big Bend
614 National Park, West Texas, U.S.A. J. Sediment. Res. 74, 391–404.
615 https://doi.org/10.1306/102203740391
616 Becker-Heidmann, P., Andresen, O., Kalmar, D., Scharpenseel, H.W., Yaalon, D.H., 2002. Carbon
617 dynamics in Vertisols as revealed by high-resolution sampling. Radiocarbon 44, 63–73.
618 https://doi.org/10.1017/S0033822200064687
619 Benvenuti, M., Bonini, M., Moratti, G., Ricci, M., Tanini, C., 2008. Tectonic and climatic controls on

historical landscape modifications: The avulsion of the lower Cecina River (Tuscany, central Italy). Geomorphology 100, 269–284. https://doi.org/10.1016/j.geomorph.2007.12.009

Blum, M.D., Törnqvist, T.E., 2000. Fluvial responses to climate and sea-level change: A review and look forward. Sedimentology 47, 2–48. https://doi.org/10.1046/j.1365-3091.2000.00008.x

Blum, M., Martin, J., Milliken, K., Garvin, M., 2013. Paleovalley systems: Insights from Quaternary analogs and experiments. Earth-Science Rev. 116, 128–169. https://doi.org/10.1016/j.earscirev.2012.09.003

Bohacs, K., Suter, J., 1997. Sequence stratigraphic distribution of coaly rocks: Fundamental controls and paralic examples. Am. Assoc. Pet. Geol. Bull. 81, 1612–1639. https://doi.org/10.1306/7834e192-1721-11d7-8645000102c1865d

Bond, G., Heinrich, H., Broecker, W., Labeyrie, L., McManus, J., 1992. andrews J. Huon S., Jantschik R., clasen S., Simet ch., Tedesco K., Klas M., Bonani G. Ivy S 245–249.

Bond, G., Broecker, W., Johnsen, S., McManus, J., Labeyrie, L., Jouzel, J., Bonanl, G., 1993. Bond 1993. Nature 365, 143–147.

Bond, G., Showers, W., Cheseby, M., Lotti, R., Almasi, P., DeMenocal, P., Priore, P., Cullen, H., Hajdas, I., Bonani, G., 1997. A pervasive millennial-scale cycle in North Atlantic Holocene and glacial climates. Science (80-. ). 278, 1257–1266.

Boul, S.W., Southard, R.J., Graham, R.C., McDaniel, P.A., 2011. Soil genesis and classification: Hoboken, 6th ed. Wiley-Blackwell, Chichester. https://doi.org/10.1002/9780470960622.

Briant, R.M., Bateman, M.D., Coope, G.R., Gibbard, P.L., 2005. Climatic control on quaternary fluvial sedimentology of a Fenland Basin river, England. Sedimentology 52, 1397–1423. https://doi.org/10.1111/j.1365-3091.2005.00747.x

Bruno, L., Amorosi, A., Curina, R., Severi, P., Bitelli, R., 2013. Human-landscape interactions in the Bologna area (northern Italy) during the mid-late Holocene, with focus on the Roman period.

644 Holocene 23, 1560–1571. https://doi.org/10.1177/0959683613499054
645 Bruno, L., Amorosi, A., Severi, P., Bartolomei, P., 2015. High-frequency depositional cycles within
646 the late Quaternary alluvial succession of Reno River (Northern Italy). Ital. J. Geosci. 134, 339–
647 354. https://doi.org/10.3301/IJG.2014.49
648 Bruno, L., Bohacs, K.M., Campo, B., Drexler, T.M., Rossi, V., Sammartino, I., Scarponi, D., Hong, W.,
649 Amorosi, A., 2017. Early Holocene transgressive palaeogeography in the Po coastal plain
650 (northern Italy). Sedimentology 64, 1792–1816. https://doi.org/10.1111/sed.12374
651 Bruno, L., Piccin, A., Sammartino, I., Amorosi, A., 2018. Decoupled geomorphic and sedimentary
652 response of Po River and its Alpine tributaries during the last glacial/post-glacial episode.
653 Geomorphology 317, 184–198. https://doi.org/10.1016/j.geomorph.2018.05.027
654 Bruno, L., Campo, B., Di Martino, A., Hong, W., Amorosi, A., 2019. Peat layer accumulation and
655 post-burial deformation during the mid-late Holocene in the Po coastal plain (Northern Italy).
656 Basin Res. 31, 621–639. https://doi.org/10.1111/bre.12339
657 Bruno, L., Campo, B., Costagli, B., Stouthamer, E., Teatini, P., Zoccarato, C., Amorosi, A., 2020a.
658 Factors controlling natural subsidence in the Po Plain. Proc. Int. Assoc. Hydrol. Sci. 382, 285–
659 290. https://doi.org/10.5194/piahs-382-285-2020
660 Bruno, L., Marchi, M., Bertolini, I., Gottardi, G., Amorosi, A., 2020b. Climate control on stacked
661 paleosols in the Pleistocene of the Po Basin (northern Italy). J. Quat. Sci. 35, 559–571.
662 https://doi.org/10.1002/jqs.3199
663 Burrato, P., Ciucci, F., Valensise, G., 2003. An inventory of river anomalies in the Po Plain, Northern
664 Italy: Evidence for active blind thrust faulting. Ann. Geophys. 46, 865–882.
665 https://doi.org/10.4401/ag-3459
666 Cacciari, M., Cremonini, S., Marchesini, M., Vianello, G., Antisari, L.V., 2017. When a pedomarker is
667 lacking: palynological and chemical multianalysis of a lateglacial-holocene soils suite

(Bologna). EQA-International J. Environ. Qual. 24, 47–73.

Cacciari, M., Amorosi, A., Marchesini, M., Kaniewski, D., Bruno, L., Campo, B., Rossi, V., 2020. Linking Holocene vegetation dynamics , palaeoclimate variability and depositional patterns in coastal successions : Insights from the Po Delta plain of northern Italy. Palaeogeogr. Palaeoclimatol. Palaeoecol. 538, 109468. https://doi.org/10.1016/j.palaeo.2019.109468

Campo, B., Amorosi, A., Bruno, L., 2016. Contrasting alluvial architecture of Late Pleistocene and Holocene deposits along a 120-km transect from the central Po Plain (northern Italy). Sediment. Geol. 341, 265–275.

Campo, B., Bruno, L., Amorosi, A., 2020. Basin-scale stratigraphic correlation of late Pleistocene-Holocene (MIS 5e-MIS 1) strata across the rapidly subsiding Po Basin (northern Italy). Quat. Sci. Rev. 237, 106300. https://doi.org/10.1016/j.quascirev.2020.106300

Chappell, J., 2002. Sea level changes forced ice breakouts in the Last Glacial cycle: New results from coral terraces. Quat. Sci. Rev. 21, 1229–1240. https://doi.org/10.1016/S0277-3791(01)00141-X

Chen, S., Huang, Y., Zou, J., Shi, Y., 2013. Mean residence time of global topsoil organic carbon depends on temperature, precipitation and soil nitrogen. Glob. Planet. Change 100, 99–108. https://doi.org/10.1016/j.gloplacha.2012.10.006

Chichagova, O.A., Cherkinsky, A.E., 1993. Problems in radiocarbon dating of soils. Radiocarbon 35, 351–362. https://doi.org/10.1017/S0033822200060355

Choi, K., 2005. Pedogenesis of late Quaternary deposits, northern Kyonggi Bay, Korea: Implications for relative sea-level change and regional stratigraphic correlation. Palaeogeogr. Palaeoclimatol. Palaeoecol. 220, 387–404. https://doi.org/10.1016/j.palaeo.2005.02.006

Clark, P.U., Huybers, P., 2009. Global change: Interglacial and future sea level. Nature 462, 856–857. https://doi.org/10.1038/462856a

692 Cleveland, D.M., Atchley, S.C., Nordt, L.C., 2007. Continental sequence stratigraphy of the Upper
693 Triassic (Norian-Rhaetian) chinle strata, northern New Mexico, U.S.A.: Allocyclic and
694 autocyclic origins of paleosol-bearing alluvial successions. J. Sediment. Res. 77, 909–924.
695 https://doi.org/10.2110/jsr.2007.082
696 Cohen, K.M., Gouw, M.J.P., Holten, J.P., 2003. Fluvio-deltaic floodbasin deposits recording
697 differential subsidence within a coastal prism (central Rhine-Meuse delta, the Netherlands).
698 Ned. Geogr. Stud. 40–68. https://doi.org/10.1002/9781444304350.ch17
699 Cremaschi, M., 1987. Paleosols and Vetusols in the Central Po Plain (Northern Italy): a study in
700 Quaternary geology and soil development, Unicopli. ed. Paleosols and Vetusols in the Central
701 Po Plain (Northern Italy): A Study in Quaternary Geology and Soil Development., Milano.
702 Cremaschi, M., Nicosia, C., 2012. Sub-Boreal aggradation along the Apennine margin of the Central
703 Po Plain: geomorphological and geoarchaeological aspects. Géomorphologie Reli. Process.
704 Environ. 18, 155–174.
705 Demko, T.M., Currie, B.S., Nicoll, K.A., 2004. Regional paleoclimatic and stratigraphic implications
706 of paleosols and fluvial/overbank architecture in the Morrison Formation (Upper Jurassic),
707 Western Interior, USA. Sediment. Geol. 167, 115–135.
708 https://doi.org/10.1016/j.sedgeo.2004.01.003
709 Diessel, C.F.K., 1992. Coal facies and depositional environment, in: Coal-Bearing Depositional
710 Systems. Springer, pp. 161–264.
711 Dubiel, R.F., Hasiotis, S.T., 2011. Deposystems, paleosols, and climatic variability in a continental
712 system: the Upper Triassic Chinle Formation, Colorado Plateau, USA. From River to Rock Rec.
713 Preserv. Fluv. Sediments their Subseq. Interpret. SEPM (Society Sediment. Geol. Spec. Publ.
714 97, 393–421.
715 Fantoni, R., Bersezio, R., Forcella, F., 2004. Alpine structure and deformation chronology at the

716 Southern Alps-Po Plain border in Lombardy. Boll. della Soc. Geol. Ital. 123, 463–476.
717 Feng, Y., 2009. Fundamental considerations of soil organic carbon dynamics: a new theoretical
718 framework. Soil Sci. 174, 467–481.
719 Fletcher, W.J., Sánchez Goñi, M.F., Allen, J.R.M., Cheddadi, R., Combourieu-Nebout, N., Huntley,
720 B., Lawson, I., Londeix, L., Magri, D., Margari, V., Müller, U.C., Naughton, F., Novenko, E.,
721 Roucoux, K., Tzedakis, P.C., 2010. Millennial-scale variability during the last glacial in
722 vegetation records from Europe. Quat. Sci. Rev. 29, 2839–2864.
723 https://doi.org/10.1016/j.quascirev.2009.11.015
724 Fontaine, S., Barot, S., Barré, P., Bdioui, N., Mary, B., Rumpel, C., 2007. Stability of organic carbon
725 in deep soil layers controlled by fresh carbon supply. Nature 450, 277–280.
726 https://doi.org/10.1038/nature06275
727 Fontana, A., Mozzi, P., Marchetti, M., 2014. Alluvial fans and megafans along the southern side of
728 the Alps. Sediment. Geol. 301, 150–171. https://doi.org/10.1016/j.sedgeo.2013.09.003
729 Garzanti, E., Vezzoli, G., Andò, S., 2011. Paleogeographic and paleodrainage changes during
730 Pleistocene glaciations (Po Plain, Northern Italy). Earth-Science Rev. 105, 25–48.
731 https://doi.org/10.1016/j.earscirev.2010.11.004
732 Gaudinski, J., Trumbore, S., Davidson, E., 2000. Soil carbon cycling in a temperate forest:
733 radiocarbon-based estimates of residence times, …. Biogeochemistry 51, 33–69.
734 Geyh, M.A., Roeschmann, G., Wijmstra, T.A., Middeldorp, A.A., 1983. The Unreliability of 14 C
735 Dates Obtained from Buried Sandy Podzols . Radiocarbon 25, 409–416.
736 https://doi.org/10.1017/s0033822200005695
737 Ghielmi, M., Minervini, M., Nini, C., Rogledi, S., Rossi, M., 2013. Late Miocene-Middle Pleistocene
738 sequences in the Po Plain - Northern Adriatic Sea (Italy): The stratigraphic record of
739 modification phases affecting a complex foreland basin. Mar. Pet. Geol. 42, 50–81.

https://doi.org/10.1016/j.marpetgeo.2012.11.007

Gibling, M.R., Bird, D.J., 1994. Late Carboniferous cyclothems and alluvial paleovalleys in the Sydney Basin, Nova Scotia. Geol. Soc. Am. Bull. 106, 105–117. https://doi.org/10.1130/0016-7606(1994)106<0105:LCCAAP>2.3.CO;2

Gibling, M.R., Fielding, C.R., Sinha, R., Davidson, S.K., Leleu, S., North, C.P., 2011. Alluvial valleys and alluvial sequences: towards a geomorphic assessment. From River to Rock Rec. Preserv. Fluv. Sediments Their Subseq. Interpret. SEPM, Spec. Publ. 97, 423–447.

Gile, L.H., Hawley, J.W., Grossman, R.B., 1981. Soils and geomorphology in the Basin and Range area of southern New Mexico: Guidebook to the Desert Project, New Mexico, Bureau of Mines and Mineral Resources Memoir.

Gilet-Blein, N., Marien, G., Evin, J., 1980. of and of of and. Radiocarbon 22, 919–929.

Gunderson, K.L., Pazzaglia, F.J., Picotti, V., Anastasio, D.A., Kodama, K.P., Rittenour, T., Frankel, K.F., Ponza, A., Berti, C., Negri, A., Sabbatini, A., 2014. Unraveling tectonic and climatic controls on synorogenic growth strata (Northern Apennines, Italy). Bull. Geol. Soc. Am. 126, 532–552. https://doi.org/10.1130/B30902.1

Hajek, E.A., Wolinsky, M.A., 2012. Simplified process modeling of river avulsion and alluvial architecture: Connecting models and field data. Sediment. Geol. 257–260, 1–30. https://doi.org/10.1016/j.sedgeo.2011.09.005

Helmens, K.F., 2014. The last interglacial-glacial cycle (MIS 5-2) re-examined based on long proxy records from central and northern europe. Quat. Sci. Rev. 86, 115–143. https://doi.org/10.1016/j.quascirev.2013.12.012

Hijma, M.P., Cohen, K.M., 2011. Holocene transgression of the Rhine river mouth area, The Netherlands/Southern North Sea: Palaeogeography and sequence stratigraphy. Sedimentology 58, 1453–1485. https://doi.org/10.1111/j.1365-3091.2010.01222.x

764 Hofmann, F., Reichenbacher, B., Farley, K.A., 2017. Evidence for >5 Ma paleo-exposure of an
765 Eocene–Miocene paleosol of the Bohnerz Formation, Switzerland. Earth Planet. Sci. Lett. 465,
766 168–175. https://doi.org/10.1016/j.epsl.2017.02.042
767 Holbrook, J., Schumm, S.A., 1999. Geomorphic and sedimentary response of rivers to tectonic
768 deformation: A brief review and critique of a tool for recognizing subtle epeirogenic
769 deformation in modern and ancient settings. Tectonophysics 305, 287–306.
770 https://doi.org/10.1016/S0040-1951(99)00011-6
771 Hošek, J., Lisá, L., Hambach, U., Petr, L., Vejrostová, L., Bajer, A., Grygar, T.M., Moska, P., Gottvald,
772 Z., Horsák, M., 2017. Middle Pleniglacial pedogenesis on the northwestern edge of the
773 Carpathian basin: A multidisciplinary investigation of the Bíňa pedo-sedimentary section, SW
774 Slovakia. Palaeogeogr. Palaeoclimatol. Palaeoecol. 487, 321–339.
775 https://doi.org/10.1016/j.palaeo.2017.09.017
776 Ishii, Y., Hori, K., Momohara, A., Nakanishi, T., Hong, W., 2016. Middle to late-Holocene decreased
777 fluvial aggradation and widespread peat initiation in the Ishikari lowland (northern Japan).
778 The Holocene 26, 1924–1938.
779 Janssens, M.M., Kasse, C., Bohncke, S.J.P., Greaves, H., Cohen, K.M., Wallinga, J., Hoek, W.Z., 2012.
780 Climate-driven fluvial development and valley abandonment at the last glacial-interglacial
781 transition (Oude IJssel-Rhine, Germany). Geol. en Mijnbouw/Netherlands J. Geosci. 91, 37–
782 62. https://doi.org/10.1017/s001677460000055x
783 Kaiser, K., Hilgers, A., Schlaak, N., Jankowski, M., Kühn, P., Bussemer, S., Przegietka, K., 2009.
784 Palaeopedological marker horizons in northern central Europe: Characteristics of Lateglacial
785 Usselo and Finow soils. Boreas 38, 591–609. https://doi.org/10.1111/j.1502-
786 3885.2008.00076.x
787 Kalisz, B., Lachacz, A., Glazewski, R., 2010. Transformation of some organic matter components in

788 organic soils exposed to drainage. Turkish J. Agric. For. 34, 245–256.
789 https://doi.org/10.3906/tar-0905-33
790 Kleber, M., 2010. What is recalcitrant soil organic matter? Environ. Chem. 7, 320–332.
791 https://doi.org/10.1071/EN10006
792 Kosters, E.C., Suter, J.R., 1993. Facies relationships and systems tracts in the late Holocene
793 Mississippi Delta Plain. J. Sediment. Petrol. 63, 727–733. https://doi.org/10.1306/D4267BCC-
794 2B26-11D7-8648000102C1865D
795 Kraus, M.J., 1999. Paleosols in clastic sedimentary rocks: Their geologic applications. Earth Sci. Rev.
796 47, 41–70. https://doi.org/10.1016/S0012-8252(99)00026-4
797 Kraus, M.J., Bown, T.M., 1993. Palaeosols and sandbody prediction in alluvial sequences. Geol.
798 Soc. London, Spec. Publ. 73, 23–31.
799 Kvale, E.P., Archer, A.W., 2007. Paleovalley fills: Trunk vs. tributary. Am. Assoc. Pet. Geol. Bull. 91,
800 809–821. https://doi.org/10.1306/11060606022
801 Lambeck, K., Antonioli, F., Anzidei, M., Ferranti, L., Leoni, G., Scicchitano, G., Silenzi, S., 2011. Sea
802 level change along the Italian coast during the Holocene and projections for the future. Quat.
803 Int. 232, 250–257. https://doi.org/10.1016/j.quaint.2010.04.026
804 Larionova, A.A., Maltseva, A.N., Lopes de Gerenyu, V.O., Kvitkina, A.K., Bykhovets, S.S., Zolotareva,
805 B.N., Kudeyarov, V.N., 2017. Effect of temperature and moisture on the mineralization and
806 humification of leaf litter in a model incubation experiment. Eurasian Soil Sci. 50, 422–431.
807 https://doi.org/10.1134/S1064229317020089
808 Lewis, S.G., Maddy, D., Scaife, R.G., 2001. The fluvial system response to abrupt climate change
809 during the last cold stage: The Upper Pleistocene River Thames fluvial succession at Ashton
810 Keynes, UK. Glob. Planet. Change 28, 341–359. https://doi.org/10.1016/S0921-
811 8181(00)00083-7

812 Machette, M.N., 1985. Calcific soils of the southwestern United States. Soils Quat. Geol.
813 Southwest. United States Geol. Soc. Am. Spec. Pap. 203, 1–21.
814 Maestrelli, D., Benvenuti, M., Bonini, M., Carnicelli, S., Piccardi, L., Sani, F., 2018. The structural
815 hinge of a chain-foreland basin: Quaternary activity of the Pede-Apennine Thrust front
816 (Northern Italy). Tectonophysics 723, 117–135. https://doi.org/10.1016/j.tecto.2017.12.006
817 Magri, D., 1999. Late Quaternary vegetation history at Lagaccione near Lago di Bolsena (central
818 Italy). Rev. Palaeobot. Palynol. 106, 171–208. https://doi.org/10.1016/S0034-6667(99)00006-
819 8
820 Marabini, S., Vai G.B., 2020. Carta Geologica della Pianura tra Imola e Ravenna, Thèodolite Editore,
821 Imola, 81pp. (in Italian).
822 Martin, C.W., Johnson, W.C., 1995. Variation in radiocarbon ages of soil organic matter fractions
823 from late Quaternary buried soils. Quat. Res. 43, 232–237.
824 Matthews, J.A., 1980. Some Problems and Implications of 14C Dates from a Podzol Buried beneath
825 an End Moraine at Haugabreen , Southern Norway Author ( s ): John A . Matthews Published
826 by : Taylor & Francis , Ltd . on behalf of the Swedish Society for Anthropology and Geography
827 62, 185–208.
828 Matthews, J.A., 1981. Natural 14 C age/depth gradient in a buried soil. Naturwissenschaften 68,
829 472–474.
830 Matthews, J.A., Dresser, P.Q., 1983. Intensive 14C dating of a buried palaeosol horizon. Geol.
831 Föreningen i Stock. Förhandlingar 105, 59–63.
832 McCarthy, P.J., Plint, A.G., 1998. Recognition of interfluve sequence boundaries: integrating
833 paleopedology and sequence stratigraphy. Geology 26, 387–390.
834 https://doi.org/10.1130/0091-7613(1998)026<0387:ROISBI>2.3.CO;2
835 McCarthy, P.J., Plint, A.G., 2003. Spatial variability of palaeosols across Cretaceous interfluves in

836 the Dunvegan Formation, NE British Columbia, Canada: Palaeohydrological,
837 palaeogeomorphological and stratigraphic implications. Sedimentology 50, 1187–1220.
838 https://doi.org/10.1111/j.1365-3091.2003.00600.x
839 Meingast, K.M., Grunert, B.K., Green, S.A., Kane, E.S., Khademimoshgenani, N., 2020. Insights on
840 dissolved organic matter production revealed by removal of charge-transfer interactions in
841 senescent leaf leachates. Water (Switzerland) 12. https://doi.org/10.3390/W12092356
842 Miall, A.D., 1985. Architectural-element analysis: a new method of facies analysis applied to fluvial
843 deposits. Earth-Science Rev. 22, 261–308.
844 Moine, O., Antoine, P., Hatté, C., Landais, A., Mathieu, J., Prud'homme, C., Rousseau, D.D., 2017.
845 The impact of Last Glacial climate variability in west-European loess revealed by radiocarbon
846 dating of fossil earthworm granules. Proc. Natl. Acad. Sci. U. S. A. 114, 6209–6214.
847 https://doi.org/10.1073/pnas.1614751114
848 Mol, J., 1997. Fluvial response to Weichselian climate changes in the Niederlausitz (Germany). J.
849 Quat. Sci. 12, 43–60. https://doi.org/10.1002/(SICI)1099-1417(199701/02)12:1<43::AID-
850 JQS291>3.0.CO;2-0
851 Monegato, G., Scardia, G., Hajdas, I., Rizzini, F., Piccin, A., 2017. The Alpine LGM in the boreal ice-
852 sheets game. Sci. Rep. 7, 1–8. https://doi.org/10.1038/s41598-017-02148-7
853 Morelli, A., Bruno, L., Cleveland, D.M., Drexler, T.M., Amorosi, A., 2017. Reconstructing Last Glacial
854 Maximum and Younger Dryas paleolandscapes through subsurface paleosol stratigraphy: An
855 example from the Po coastal plain, Italy. Geomorphology 295, 790–800.
856 https://doi.org/10.1016/j.geomorph.2017.08.013
857 Mozzi, P., Bini, C., Zilocchi, L., Becattini, R., Lippi, M.M., 2003. Stratigraphy, palaeopedology and
858 palynology of late Pleistocene and Holocene deposits in the landward sector of the Lagoon of
859 Venice (Italy), in relation to the Caranto level. Alp. Mediterr. Quat. 16, 193–210.

Muttoni, G., Carcano, C., Garzanti, E., Ghielmi, M., Piccin, A., Pini, R., Rogledi, S., Sciunnach, D., 2003. Onset of major Pleistocene glaciations in the Alps. Geology 31, 989–992. https://doi.org/10.1130/G19445.1

Muttoni, G., Scardia, G., Kent, D. V., Morsiani, E., Tremolada, F., Cremaschi, M., Peretto, C., 2011. First dated human occupation of Italy at ~0.85Ma during the late Early Pleistocene climate transition. Earth Planet. Sci. Lett. 307, 241–252. https://doi.org/10.1016/j.epsl.2011.05.025

Orlova, L.A., Panychev, V.A., 1993. The reliability of radiocarbon dating buried soils. Radiocarbon 35, 369–377. https://doi.org/10.1017/S0033822200060379

Pandey, D., Agrawal, M., Singh Bohra, J., Adhya, T.K., Bhattacharyya, P., 2014. Recalcitrant and labile carbon pools in a sub-humid tropical soil under different tillage combinations: A case study of rice-wheat system. Soil Tillage Res. 143, 116–122. https://doi.org/10.1016/j.still.2014.06.001

Pati, P., Verma, A.K., Dash, C., Patel, N.K., Gupta, A., Sharma, V., Jakhmola, R.P., Parkash, B., Awasthi, A.K., Saraf, A.K., 2019. Influence of neotectonism on geomorphology and depositional architecture of the Gandak megafan, middle Ganga plain, India. Geomorphology 327, 489–503. https://doi.org/10.1016/j.geomorph.2018.11.029

Pellegrini, C., Asioli, A., Bohacs, K.M., Drexler, T.M., Feldman, H.R., Sweet, M.L., Maselli, V., Rovere, M., Gamberi, F., Valle, G.D., Trincardi, F., 2018. The late Pleistocene Po River lowstand wedge in the Adriatic Sea: Controls on architecture variability and sediment partitioning. Mar. Pet. Geol. 96, 16–50. https://doi.org/10.1016/j.marpetgeo.2018.03.002

Peltier, W.R., Fairbanks, R.G., 2006. Global glacial ice volume and Last Glacial Maximum duration from an extended Barbados sea level record. Quat. Sci. Rev. 25, 3322–3337. https://doi.org/10.1016/j.quascirev.2006.04.010

Phillips, J.D., 2011. Universal and local controls of avulsions in southeast Texas Rivers.

884 Geomorphology 130, 17–28. https://doi.org/10.1016/j.geomorph.2010.10.001
885 Picotti, V., Pazzaglia, F.J., 2008. A new active tectonic model for the construction of the Northern
886 Apennines mountain front near Bologna (Italy). J. Geophys. Res. Solid Earth 113, 1–24.
887 https://doi.org/10.1029/2007JB005307
888 Pini, R., Ravazzi, C., Reimer, P.J., 2010. The vegetation and climate history of the last glacial cycle in
889 a new pollen record from Lake Fimon (southern Alpine foreland, N-Italy). Quat. Sci. Rev. 29,
890 3115–3137. https://doi.org/10.1016/j.quascirev.2010.06.040
891 Piovan, S., Mozzi, P., Zecchin, M., 2012. The interplay between adjacent Adige and Po alluvial
892 systems and deltas in the late Holocene (Northern Italy). Géomorphologie Reli. Process.
893 Environ. 18, 427–440.
894 Plint, A.G., Moore, J., Plint, A., Sanders, J., Ulic, D., 2001. stratigraphy : Updip expression Formation
895 , Alberta foreland. October 11, 1967–2001.
896 Rasbury, E.T., Hanson, G.N., Meyers, W.J., Saller, A.H., 1997. Dating of the time of sedimentation
897 using U-Pb ages for paleosol calcite. Geochim. Cosmochim. Acta 61, 1525–1529.
898 https://doi.org/10.1016/S0016-7037(97)00043-4
899 Rasmussen, S.O., Bigler, M., Blockley, S.P., Blunier, T., Buchardt, S.L., Clausen, H.B., Cvijanovic, I.,
900 Dahl-Jensen, D., Johnsen, S.J., Fischer, H., Gkinis, V., Guillevic, M., Hoek, W.Z., Lowe, J.J.,
901 Pedro, J.B., Popp, T., Seierstad, I.K., Steffensen, J.P., Svensson, A.M., Vallelonga, P., Vinther,
902 B.M., Walker, M.J.C., Wheatley, J.J., Winstrup, M., 2014. A stratigraphic framework for abrupt
903 climatic changes during the Last Glacial period based on three synchronized Greenland ice-
904 core records: Refining and extending the INTIMATE event stratigraphy. Quat. Sci. Rev. 106,
905 14–28. https://doi.org/10.1016/j.quascirev.2014.09.007
906 Ravazzi, C., Donegana, M., Vescovi, E., Arpenti, E., Caccianiga, M., Kaltenrieder, P., Londeix, L.,
907 Marabini, S., Mariani, S., Pini, R., Vai, G.B., Wick, L., 2006. A new Late-glacial site with Picea

abies in the northern Apennine foothills: An exception to the model of glacial refugia of trees. Veg. Hist. Archaeobot. 15, 357–371. https://doi.org/10.1007/s00334-006-0055-9

Ravazzi, C., Deaddis, M., De Amicis, M., Marchetti, M., Vezzoli, G., Zanchi, A., 2012. Évolution de la plaine centrale du Pô entre les rivières Adda et Serio au cours des 40 derniers millénaires. Geomorphol. Reli. Process. Environ. 131–154. https://doi.org/10.4000/geomorphologie.9794

Regione Emilia-Romagna & Eni-Agip, 1998. Riserve idriche sotterranee della Regione Emilia-Romagna. S.EL.CA, Firenze *(in Italian)*.

Reimer, P.J., Austin, W.E.N., Bard, E., Bayliss, A., Blackwell, P.G., Bronk Ramsey, C., Butzin, M., Cheng, H., Edwards, R.L., Friedrich, M., Grootes, P.M., Guilderson, T.P., Hajdas, I., Heaton, T.J., Hogg, A.G., Hughen, K.A., Kromer, B., Manning, S.W., Muscheler, R., Palmer, J.G., Pearson, C., Van Der Plicht, J., Reimer, R.W., Richards, D.A., Scott, E.M., Southon, J.R., Turney, C.S.M., Wacker, L., Adolphi, F., Büntgen, U., Capano, M., Fahrni, S.M., Fogtmann-Schulz, A., Friedrich, R., Köhler, P., Kudsk, S., Miyake, F., Olsen, J., Reinig, F., Sakamoto, M., Sookdeo, A., Talamo, S., 2020. The IntCal20 Northern Hemisphere Radiocarbon Age Calibration Curve (0-55 cal kBP). Radiocarbon 62, 725–757. https://doi.org/10.1017/RDC.2020.41

Richardson, J.L., Vepraskas, M.J., 2001. Wetland soilsgenesis, hydrology, landscapes, and classification.

Rousseau, D.D., Sima, A., Antoine, P., Hatté, C., Lang, A., Zöller, L., 2007. Link between European and North Atlantic abrupt climate changes over the last glaciation. Geophys. Res. Lett. 34, 2–7. https://doi.org/10.1029/2007GL031716

Rousseau, D.D., Antoine, P., Gerasimenko, N., Sima, A., Fuchs, M., Hatté, C., Moine, O., Zoeller, L., 2011. North Atlantic abrupt climatic events of the last glacial period recorded in Ukrainian loess deposits. Clim. Past 7, 221–234. https://doi.org/10.5194/cp-7-221-2011

Scharpenseel, H.W., 1971. Radiocarbon dating of soils--problems, troubles, hopes. Paleopedol.

Orig. Nat. Dating Paleosols. Pap. 77–88.

Shanley, K.W., McCabe, P.J., 1994. Perspectives on the sequence stratigraphy of continental strata. Am. Assoc. Pet. Geol. Bull. 78, 544–568. https://doi.org/10.1306/bdff9258-1718-11d7-8645000102c1865d

Synal, H.A., Stocker, M., and Suter, M., 2007. MICADAS: A new compact radiocarbon AMS system. Nuclear Instruments & Methods in Physics Research Section B-Beam Interactions with Materials and Atoms 259, 7-13. https://doi.org/10.1016/j.nimb.2007.01.138

Soares, M.V.T., Basilici, G., Lorenzoni, P., Colombera, L., Mountney, N.P., Martinelli, A.G., Ferreira Mesquita, Á., da Silva Marinho, T., Vásconez García, R.G., Marconato, A., 2020. Landscape and depositional controls on palaeosols of a distributive fluvial system (Upper Cretaceous, Brazil). Sediment. Geol. 410, 105774. https://doi.org/10.1016/j.sedgeo.2020.105774

Soldati, M., Borgatti, L., Cavallin, A., De Amicis, M., Frigerio, S., Giardino, M., Mortara, G., Pellegrini, G.B., Ravazzi, C., Surian, N., Tellini, C., Zanchi, A., Alberto, W., Albanese, D., Chelli, A., Corsini, A., Marchetti, M., Palomba, M., Panizza, M., 2006. Geomorphological evolution of slopes and climate changes in Northern Italy during the late quaternary: Spatial and temporal distribution of landslides and landscape sensitivity implications. Geogr. Fis. e Din. Quat. 29, 164–183.

Stolt, M.H., Rabenhorst, M.C., 2011. Introduction and historical development of subaqueous soil concepts. 36: 1-14.

Storms, J.E.A., Weltje, G.J., Terra, G.J., Cattaneo, A., Trincardi, F., 2008. Coastal dynamics under conditions of rapid sea-level rise: Late Pleistocene to Early Holocene evolution of barrier-lagoon systems on the northern Adriatic shelf (Italy). Quat. Sci. Rev. 27, 1107–1123. https://doi.org/10.1016/j.quascirev.2008.02.009

Stouthamer, E., Cohen, K.M., Gouw, M.J.P., 2011. Avulsion and its implications for fluvial-deltaic

architecture: insights from the Holocene Rhine-Meuse delta. SEPM Spec. Publ. 97, 215–232.

Synal HA, Stocker M, and Suter M. 2007. MICADAS: A new compact radiocarbon AMS system. *Nuclear Instruments & Methods in Physics Research Section B-Beam Interactions with Materials and Atoms* 259: 7-13.

Tebbens, L.A., Veldkamp, A., Westerhoff, W., Kroonenberg, S.B., 1999. Fluvial incision and channel downcutting as a response to Late-glacial and Early Holocene climate change: The lower reach of the river Meuse (Maas), The Netherlands. J. Quat. Sci. 14, 59–75. https://doi.org/10.1002/(SICI)1099-1417(199902)14:1<59::AID-JQS408>3.0.CO;2-Z

Toonen, W.H.J., Kleinhans, M.G., Cohen, K.M., 2012. Sedimentary architecture of abandoned channel fills. Earth Surf. Process. Landforms 37, 459–472. https://doi.org/10.1002/esp.3189

Törnqvist, T.E., 1993. HOLOCENE ALTERNATION OF MEANDERING AND ANASTOMOSING Formation Kreftenheye Formation m below Dutch Ordnance Datum ( O . D .) _ Twent ~ e F ~ rmation ~ Betuwe and Formation Broek Formation / T ~ wente Formation. J. Sediment. Petrol. 63, 683–693.

Trendell, A.M., Atchley, S.C., Nordt, L.C., 2012. Depositional and diagenetic controls on reservoir attributes within a fluvial outcrop analog: Upper Triassic Sonsela member of the Chinle Formation, Petrified Forest National Park, Arizona. Am. Assoc. Pet. Geol. Bull. 96, 679–707. https://doi.org/10.1306/08101111025

Tsatskin, A., Sandler, A., Avnaim-Katav, S., 2015. Quaternary subsurface paleosols in Haifa Bay, Israel: A new perspective on stratigraphic correlations in coastal settings. Palaeogeogr. Palaeoclimatol. Palaeoecol. 426, 285–296. https://doi.org/10.1016/j.palaeo.2015.03.018

van Balen, R.T., Busschers, F.S., Tucker, G.E., 2010. Modeling the response of the Rhine-Meuse fluvial system to Late Pleistocene climate change. Geomorphology 114, 440–452. https://doi.org/10.1016/j.geomorph.2009.08.007

Vandenberghe, J., 2003. Climate forcing of fluvial system development: An evolution of ideas. Quat. Sci. Rev. 22, 2053–2060. https://doi.org/10.1016/S0277-3791(03)00213-0

Vannoli, P., Burrato, P., Valensise, G., 2015. The Seismotectonics of the Po Plain (Northern Italy): Tectonic Diversity in a Blind Faulting Domain. Pure Appl. Geophys. 172, 1105–1142. https://doi.org/10.1007/s00024-014-0873-0

Vescovi, E., Ammann, B., Ravazzi, C., Tinner, W., 2010. A new Late-glacial and Holocene record of vegetation and fire history from Lago del Greppo, northern Apennines, Italy. Veg. Hist. Archaeobot. 19, 219–233. https://doi.org/10.1007/s00334-010-0243-5

Viseras, C., Calvache, M.L., Soria, J.M., Fernńdez, J., 2003. Differential features of alluvial fans controlled by tectonics or eustatic accommodation space. Examples from the Betic Cordillera, Spain. Geomorphology 50, 181–202. https://doi.org/10.1016/S0169-555X(02)00214-3

Wadsworth, J., Boyd, R., Diessel, C., Leckie, D., 2003. Stratigraphic style of coal and non-marine strata in a high accommodation setting: Falher Member and Gates Formation (Lower Cretaceous), western Canada. Bull. Can. Pet. Geol. 51, 275–303. https://doi.org/10.2113/51.3.275

Wright, V.P., Marriott, S.B., 1993. The sequence stratigraphy of fluvial depositional systems: the role of floodplain sediment storage. Sediment. Geol. 86, 203–210.

Zeeden, C., Hambach, U., Veres, D., Fitzsimmons, K., Obreht, I., Bösken, J., Lehmkuhl, F., 2018. Millennial scale climate oscillations recorded in the Lower Danube loess over the last glacial period. Palaeogeogr. Palaeoclimatol. Palaeoecol. 509, 164–181. https://doi.org/10.1016/j.palaeo.2016.12.029

Zerboni, A., Trombino, L., Frigerio, C., Livio, F., Berlusconi, A., Michetti, A.M., Rodnight, H., Spötl, C., 2015. The loess-paleosol sequence at Monte Netto: a record of climate change in the Upper Pleistocene of the central Po Plain, northern Italy. J. Soils Sediments 15, 1329–1350.

https://doi.org/10.1007/s11368-014-0932-2

Zuffetti, C., Trombino, L., Zembo, I., Bersezio, R., 2018. Soil evolution and origin of landscape in a late Quaternary tectonically mobile setting: The Po Plain-Northern Apennines border in Lombardy (Italy). Catena 171, 376–397. https://doi.org/10.1016/j.catena.2018.07.026

**Figures and captions**

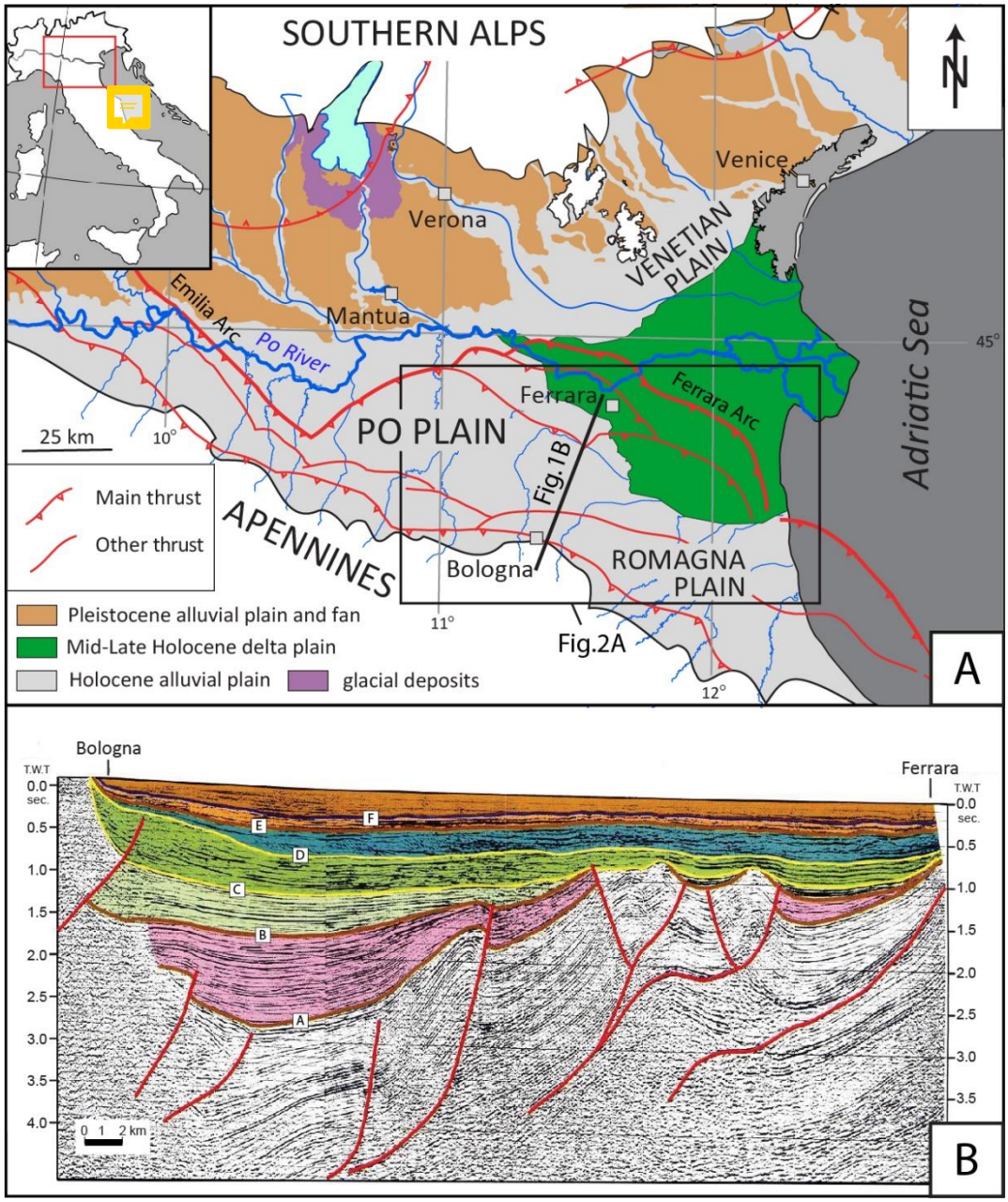

Fig. 1 – A. Geological map of the Po Plain, with location of the study area and of the seismic profile of Fig. 1B (modified after Bruno et al., 2019). The extent of Pleistocene alluvial deposits is from Fontana et al. (2014). Buried structures are modified after Burrato et al., (2003). B. Interpreted deep seismic profile (from Regione Emilia-Romagna & Eni-Agip, 1998, location in Figure 1A), with identification of the major blind thrusts (red lines) and main stratigraphic unconformities (lines from A–F) within the Po Basin fill (coloured area).

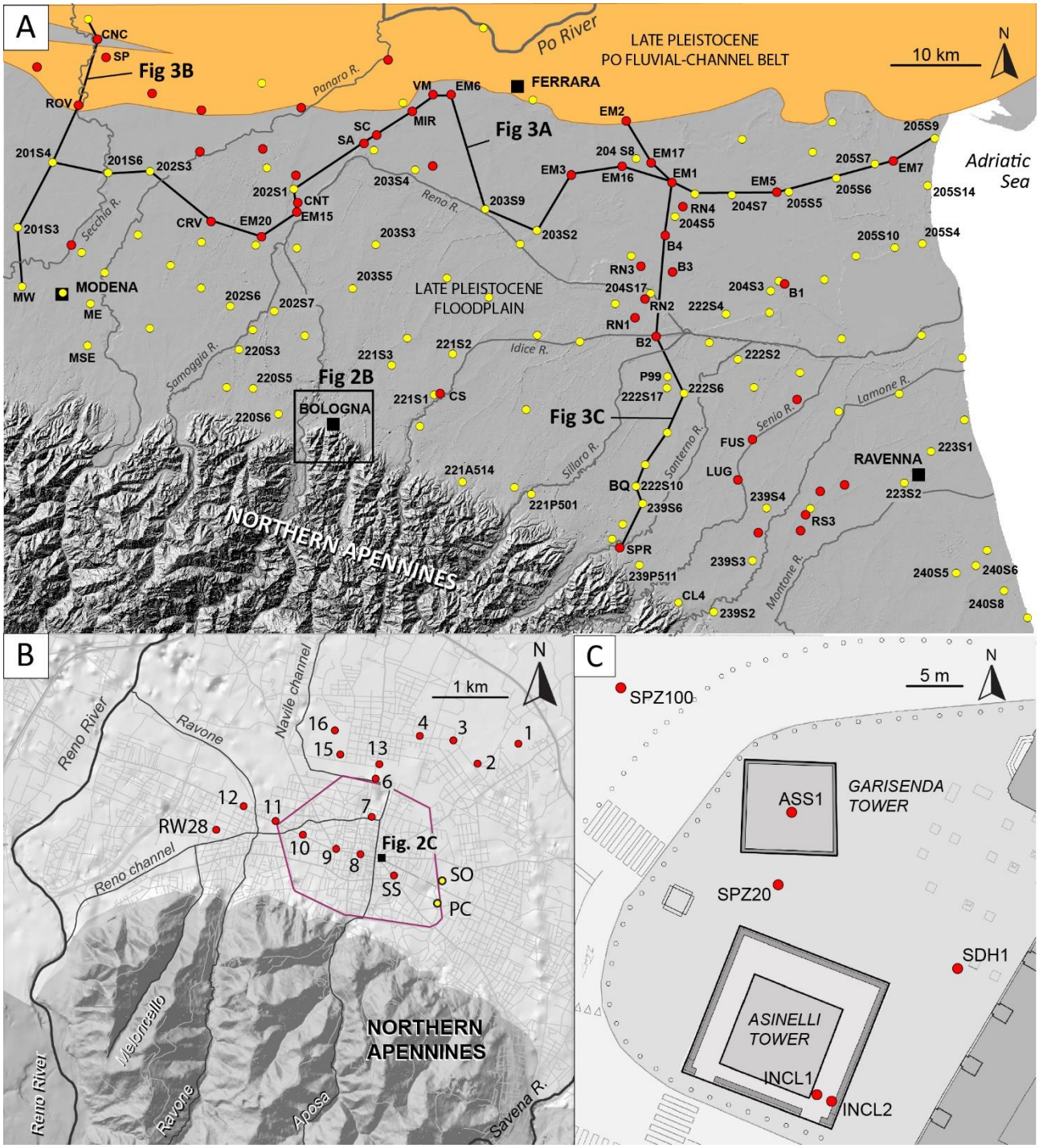


Fig. 2 – A. Study area with location of cores (red circles), core descriptions (yellow circles) and cross-sections of Fig. 5. B. Close-up on the Bologna area, with location of cores shown in Fig. 6. C. Location of cores drilled in the Two-Towers Medieval district (modified after Bruno et al., 2020b).

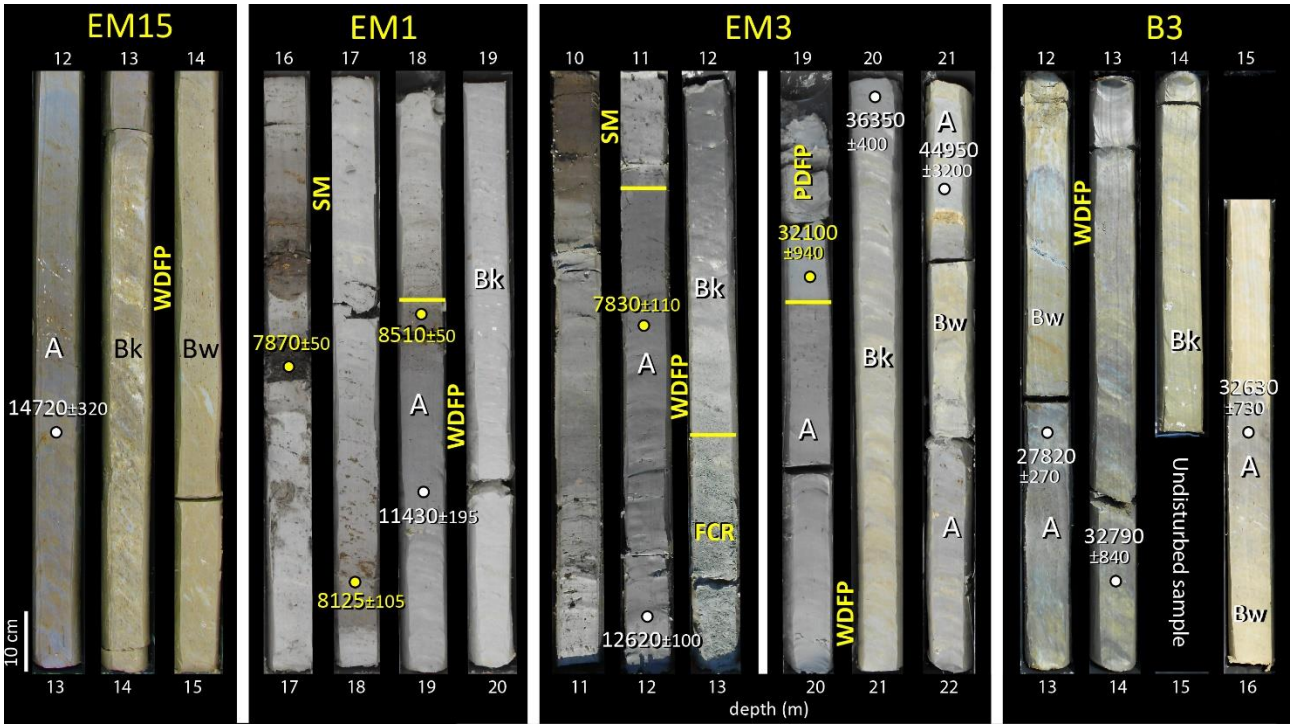


Fig. 3 – Representative photographs of paleosols from cores EM1, EM3 and B3 (location in Fig. 2). WDFP: well-drained floodplain; PDFP: poorly-drained floodplain; SW: swamp; FCR: fluvial-channel-related deposits. For pedological horizons A, Bk and Bw, see text. The white dates (cal kyr B.P.) are from bulk-sediment samples, whereas the yellow ones are from plant macrofossils.

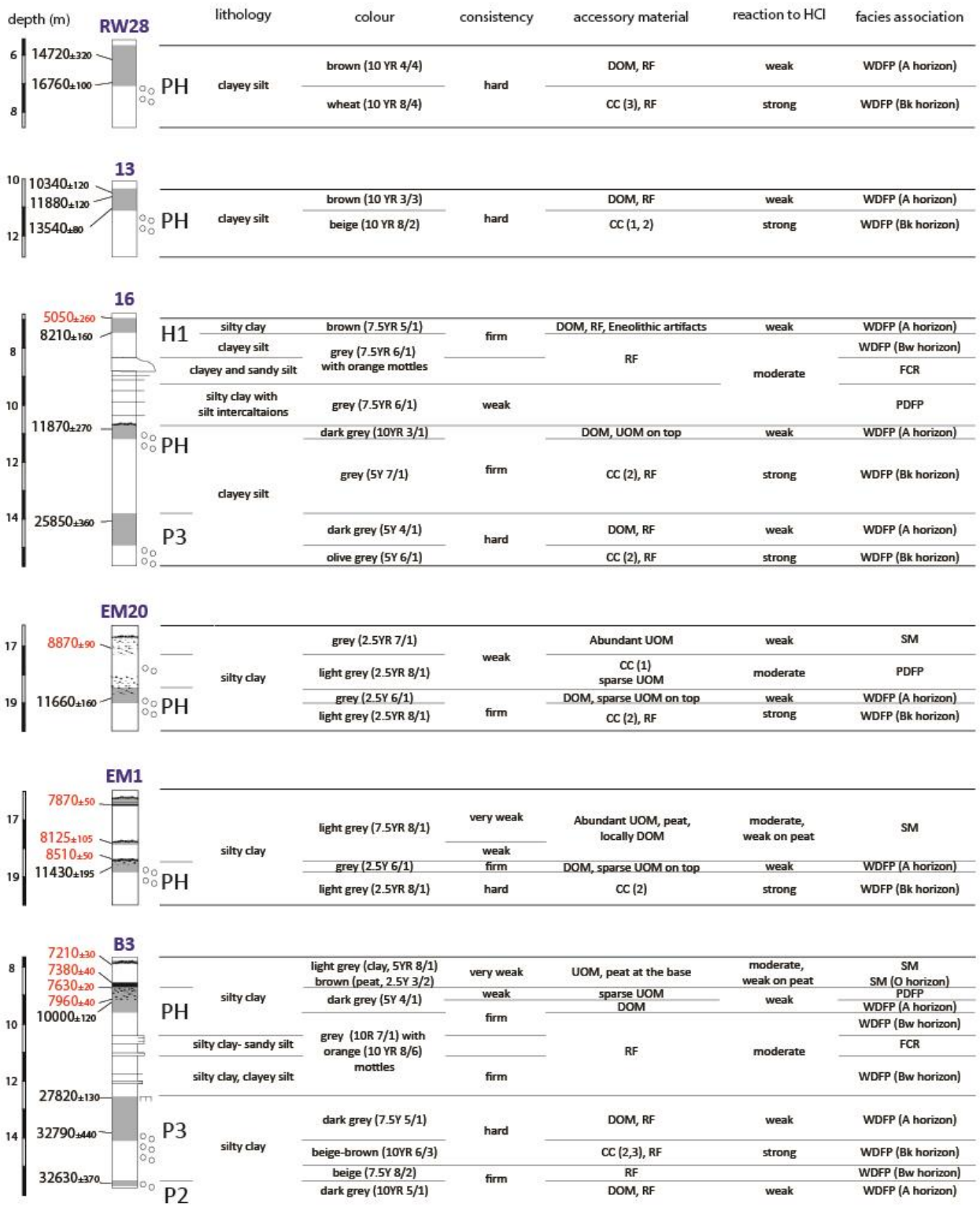


Fig. 4 – Sedimentological characters and radiocarbon ages of paleosols P2, P3, PH and H1 from cores RW28, 16, 17, EM1, EM20 and B3 (for location see Fig. 2). DOM: dissolved organic matter; UOM: undecomposed organic matter; RF: redoximorphic features; CC carbonate concretions (the number indicates the evolutionary stage, from Gile et al., 1981; Machette et al., 1985). WDFP: well-drained

floodplain; PDFP: poorly-drained floodplain; SW: swamp; FCR: fluvial-channel-related deposits. The black dates (cal kyr B.P.) are from bulk-sediment samples, whereas the red ones are from plant macrofossils.

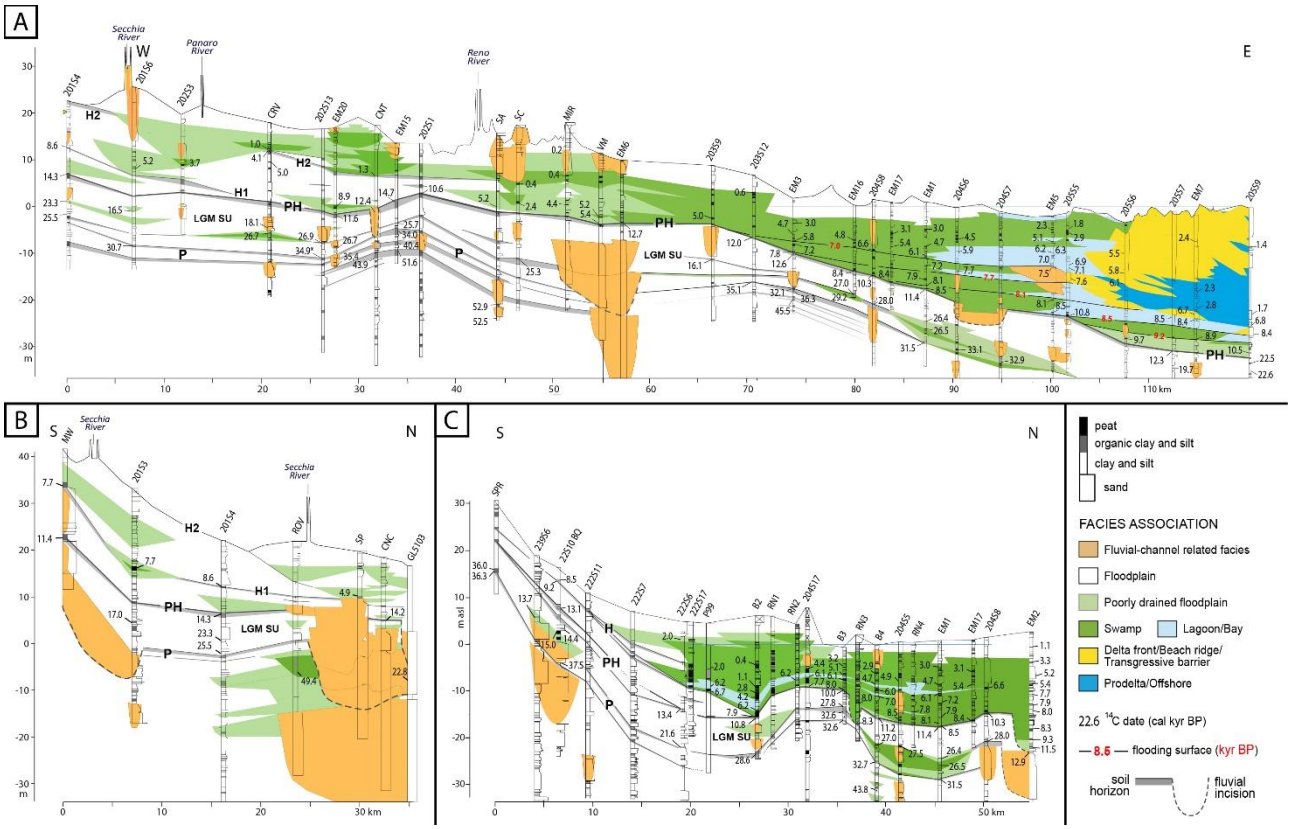


Fig. 5 – Upper Pleistocene and Holocene stratigraphy of the Po Plain depicted in cross-sections with W-E (A) and S-N (B and C) orientations (location in Fig. 2A). LGM SU: Last Glacial Maximum Stratigraphic Unit.

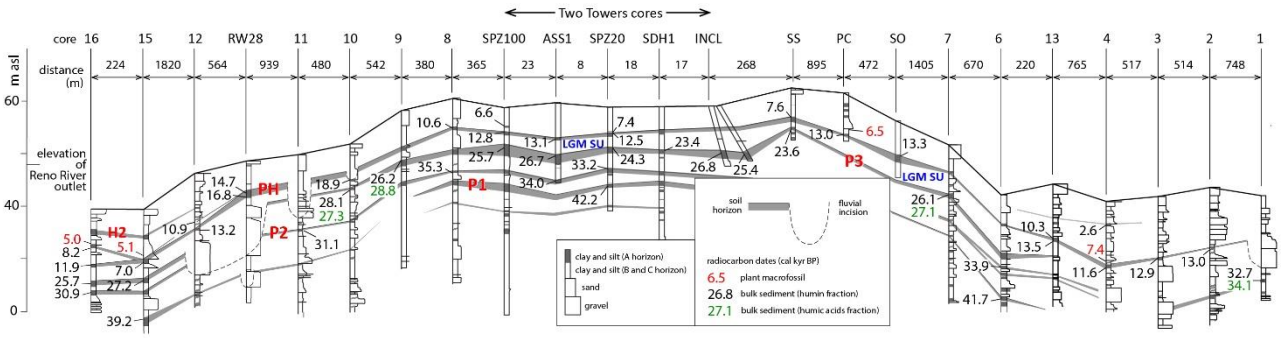


1046

1047 Fig. 6 – Paleosol-based correlations in the Bologna Area. LGM SU: Last Glacial Maximum

1048 Stratigraphic Unit. Location of cores in Fig 2.

1049

1050

1051

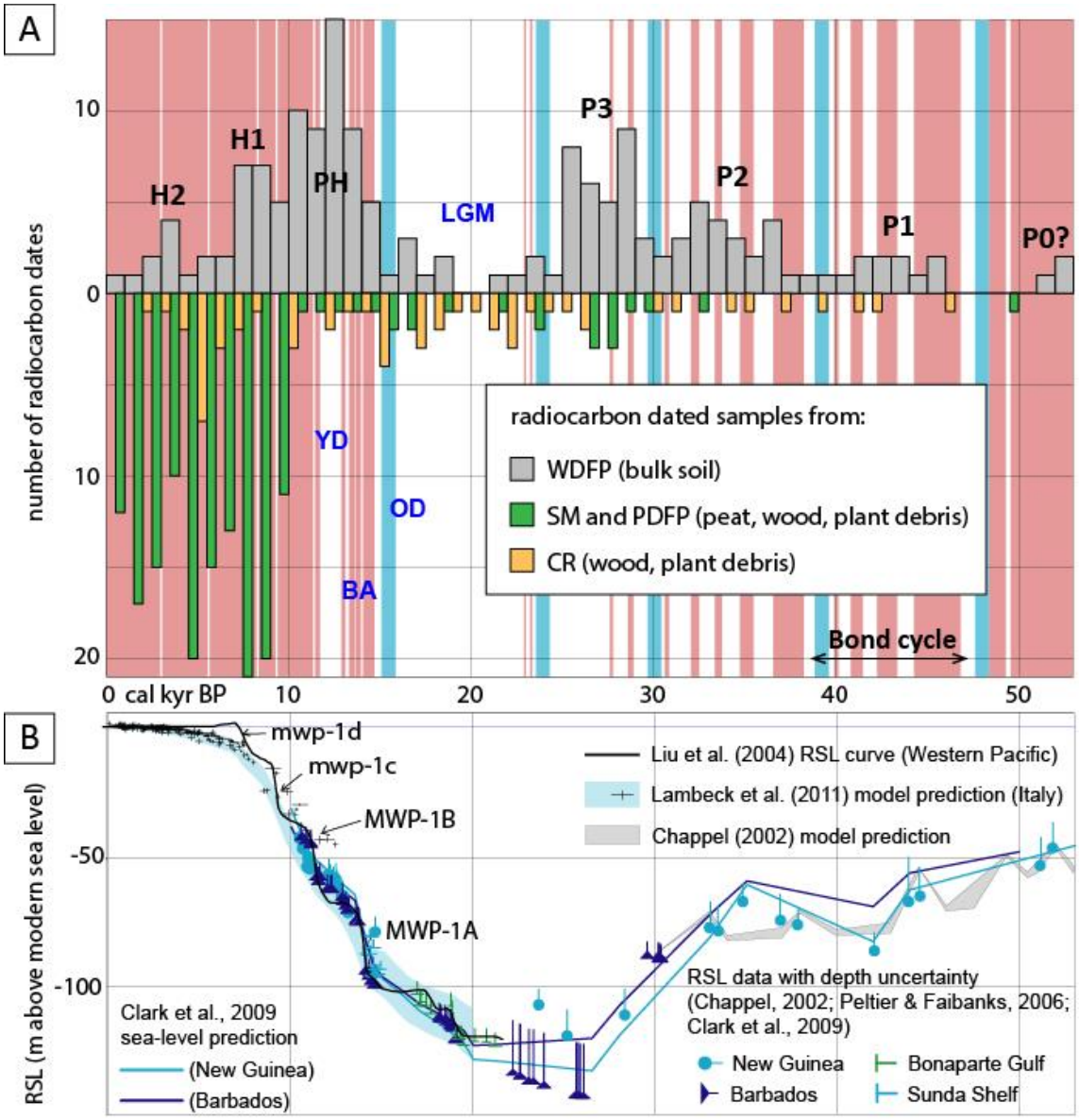


Fig. 7 – A. Distribution of radiocarbon dates from bulk-soil and plant-macrofossil samples. A major peak in dates from bulk-soil samples corresponds to paleosol PH; five minor peaks are related to paleosols P1, P2, P3, H1 and H2. Notable is the lack of radiocarbon dated soils around 20 cal ky B.P. (LGM). The sharp increase in radiocarbon dates from plant-macrofossils after 10 ky B.P., paralleled by a decline in the number of dates from bulk-soil samples, reflects the onset of estuarine-deltaic sedimentation in the distal Po Plain and the burial of paleosol PH. Red areas correspond to interstadials, according to Bond et al., (1997) and Rasmussen et al. (2014). OD: Oldest Dryas; YD: Younger Dryas. Light blue vertical bars indicate Henrich events (Bond et al., 1992). B. Sea-level oscillations during the last 50 ky.

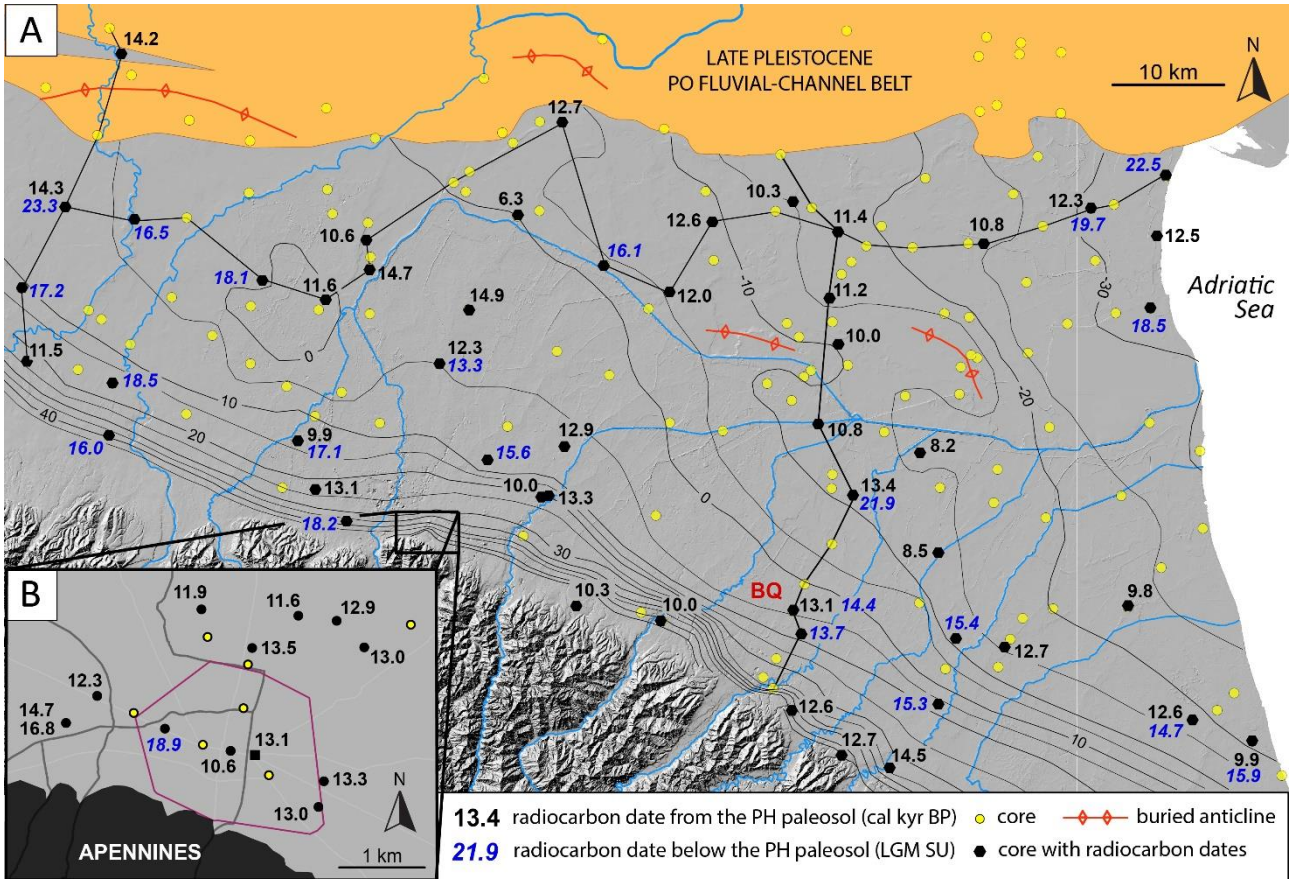


Fig. 8 – Radiocarbon dates (black numbers, cal ky B.P.) from paleosol PH (bulk soil samples) in the Po Plain (A) and in the Bologna urban area (B). Blue numbers are the youngest ages from the underlying LGM stratigraphic unit. The present-day elevation (metres above modern sea-level) of paleosol PH is depicted through 5 m-spaced isolines. BQ: Bubano Quarry.

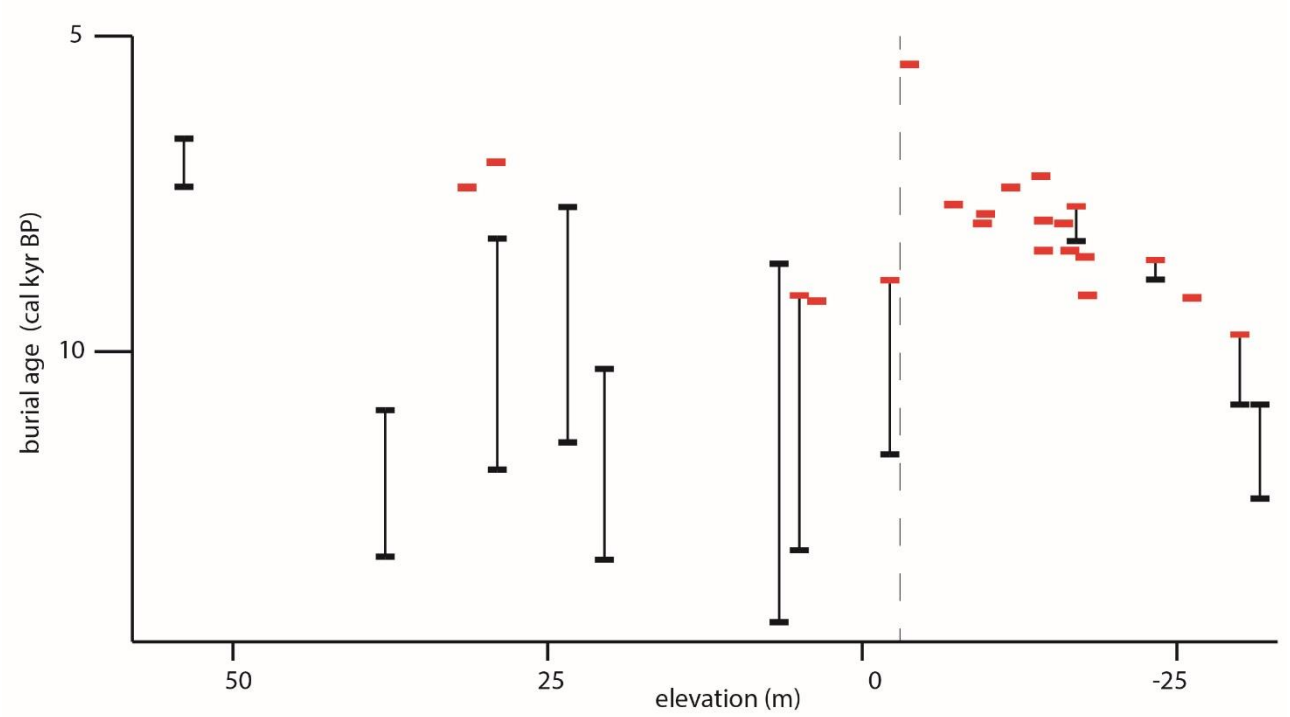


Fig. 9 – Burial ages of paleosol PH plotted against its present-day elevation (metres above modern sea-level). Black rectangles are radiocarbon dates from bulk soil samples. Red rectangles are radiocarbon dates from plant macrofossils. Burial ages from samples at elevation < - 3 m (dashed line) show an overall inverse proportionality with elevation. On the contrary, no specific trends are observable in burial-age distribution at elevation > - 3 m.

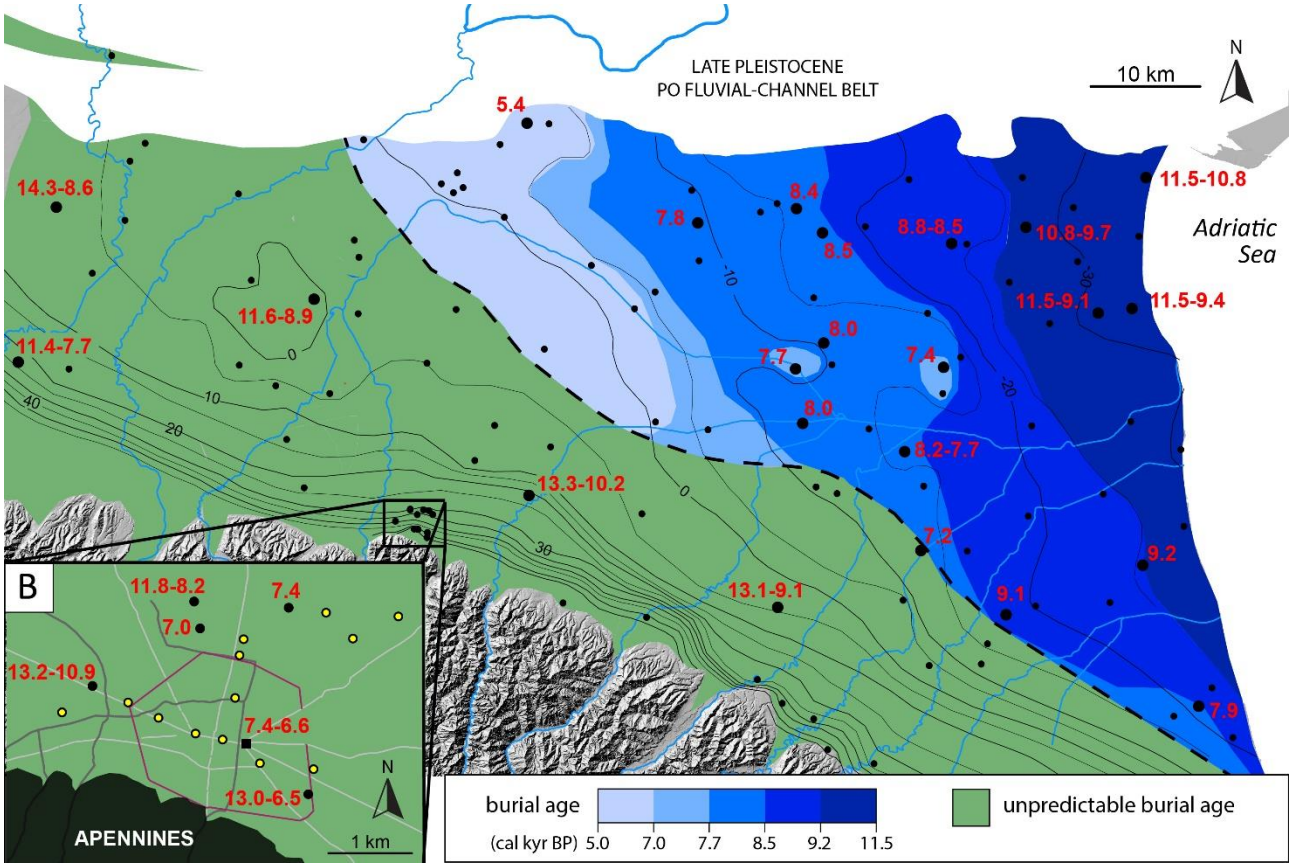


Fig. 10 – Map showing burial ages (cal kyr B.P.) of paleosol PH in the Po Plain (A) and in the Bologna urban area (B). The shades of blue depict progressively younger burial ages upland. In the green area burial ages do not show specific spatial trends. Red numbers represent burial ages or intervals measured along single cores (black circles). The map also depicts the present-day elevation (metres above modern sea-level) of paleosol PH through 5 m-spaces isolines. Black dots are the countered data points. The dashed line represents the maximum landward extent of Holocene estuarine and delta plain deposits.

Figure 1

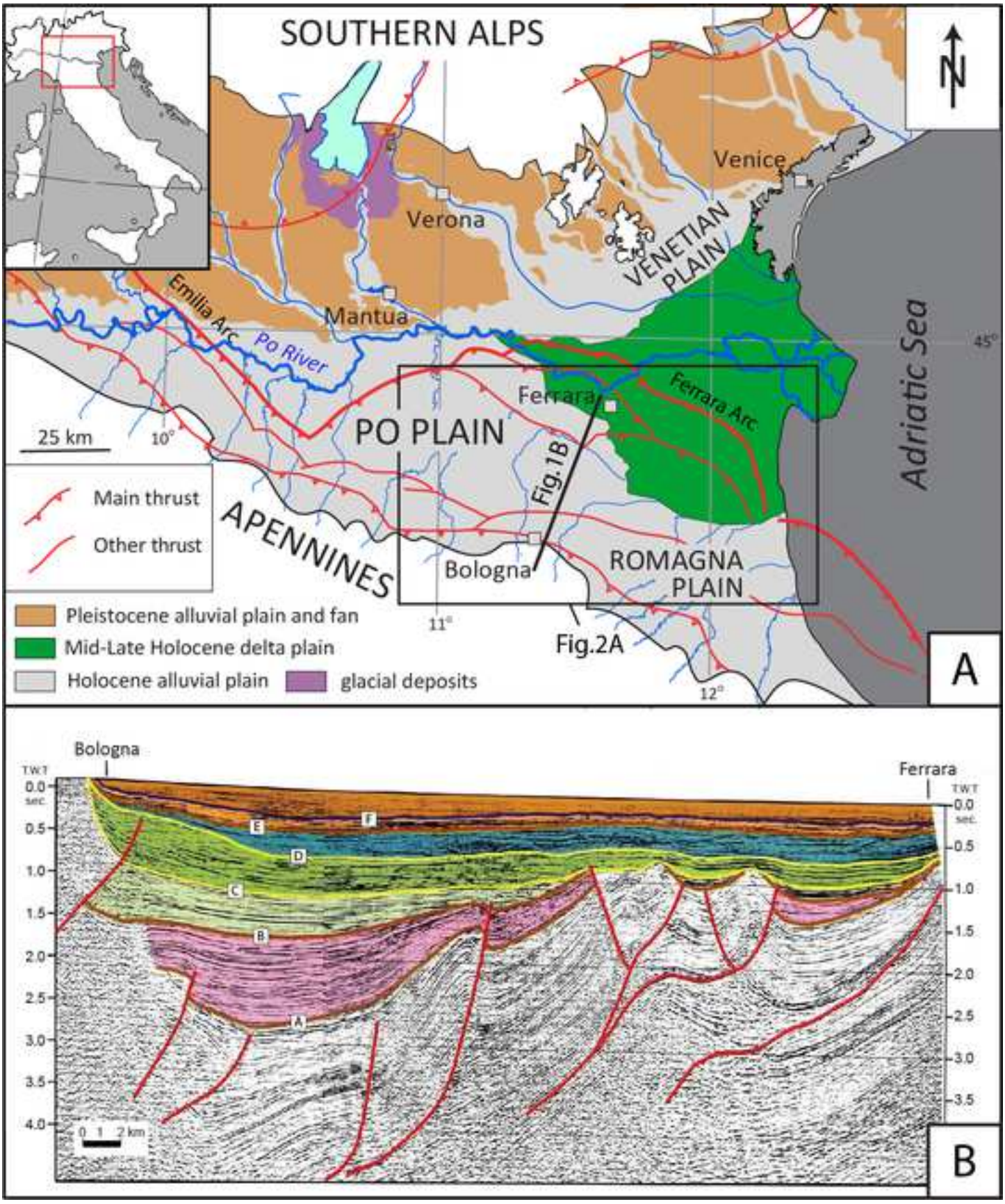
SOUTHERN ALPS
N
Venice
Verona
VENETIAN PLAIN
Emilia Arc
Po River
Mantua
Adriatic Sea
45°
Ferrara
Ferrara Arc
25 km
10°
PO PLAIN
Fig.1B
Main thrust
Other thrust
APENNINES
Bologna
ROMAGNA PLAIN
11°
Fig.2A
Pleistocene alluvial plain and fan
Mid-Late Holocene delta plain
Holocene alluvial plain
glacial deposits
12°
A
Bologna
Ferrara
TWT
0.0
sec.
0.5
1.0
1.5
2.0
2.5
3.0
3.5
4.0
F
E
D
C
B
A
0 1 2 km
B

Figure 2

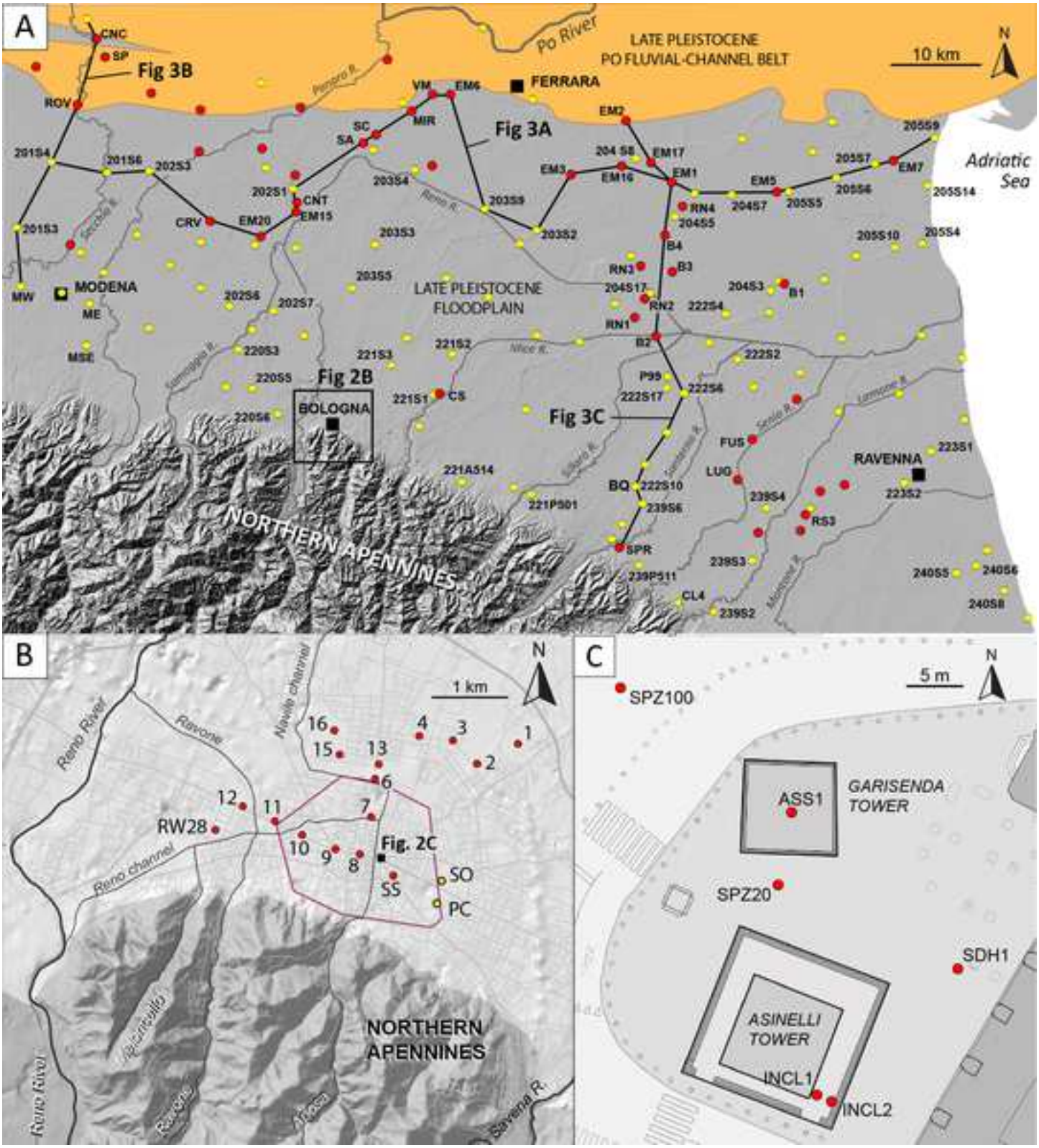
A
Po River
LATE PLEISTOCENE
PO FLUVIAL-CHANNEL BELT
10 km
N
Adriatic
Sea
Fig 3B
Fig 3A
Fig 3C
Fig 2B
FERRARA
MODENA
BOLOGNA
RAVENNA
LATE PLEISTOCENE
FLOODPLAIN
NORTHERN APENNINES
CNC
SP
ROV
VM
EM6
MIR
SC
SA
EM2
EM17
EM1
EM5
EM7
EM3
EM16
RN4
CNT
EM15
CRV
EM20
MW
ME
MSE
B4
B3
B2
B1
RN3
RN2
RN1
P99
C5
FUS
LUO
BQ
SPR
CL4
RS3
B
1 km
N
Reno River
Ravone
Navile channel
Reno channel
RW28
Fig. 2C
SO
SS
PC
NORTHERN
APENNINES
C
5 m
N
SPZ100
ASS1
GARISENDA
TOWER
SPZ20
SDH1
ASINELLI
TOWER
INCL1
INCL2

Figure 3

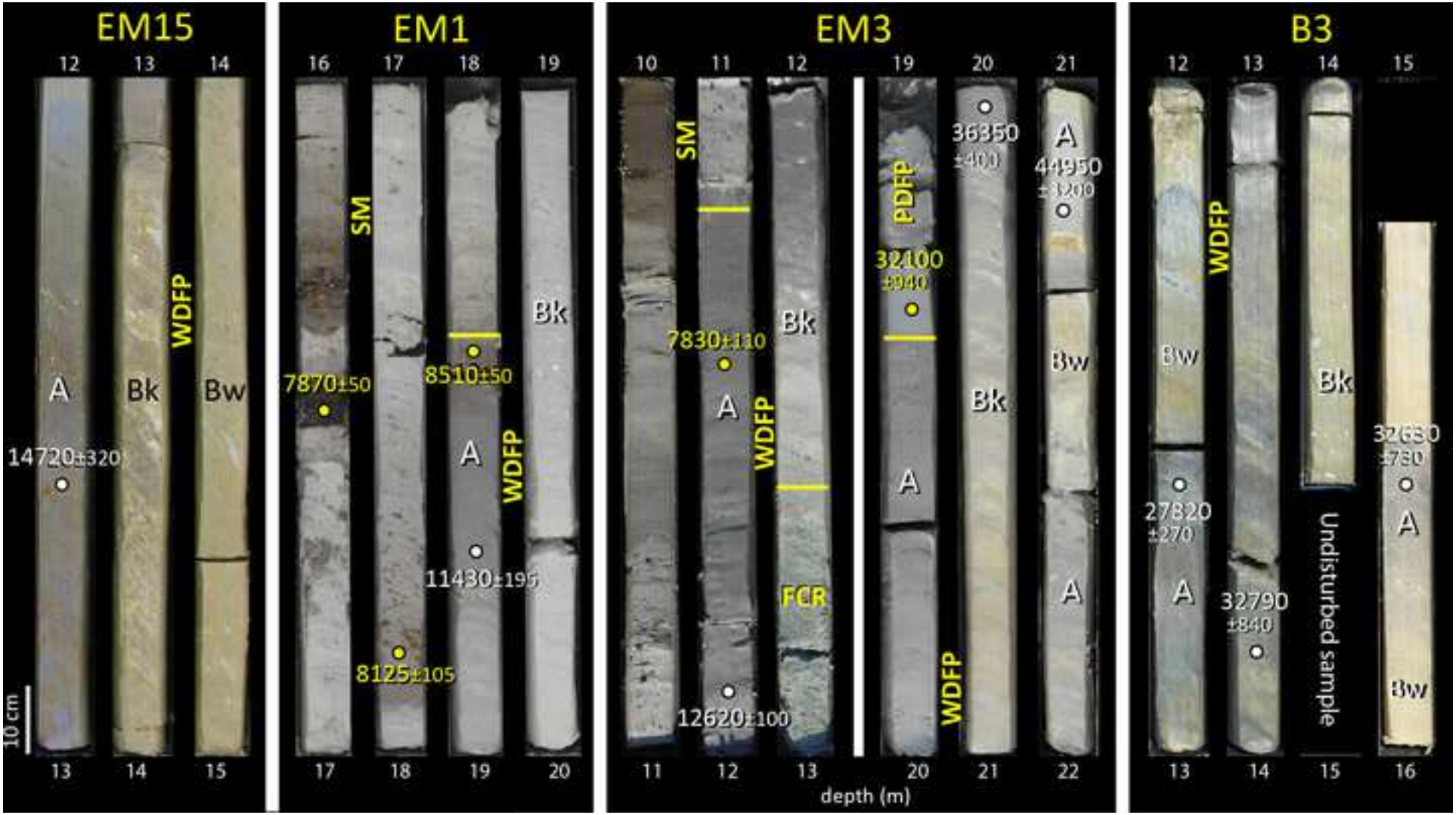
EM15
12
13
14
A
Bk
Bw
WDFP
14720±320
10 cm
13
14
15
EM1
16
17
18
19
SM
7870±50
8510±50
Bk
A
WDFP
11430±195
8125±105
17
18
19
20
EM3
10
11
12
19
20
21
SM
7830±110
Bk
A
WDFP
FCR
12620±100
PDFP
32100
±940
36350
±400
A
44950
±3200
Bk
Bw
A
WDFP
11
12
13
20
21
22
depth (m)
B3
12
13
14
15
WDFP
Bw
27820
±270
A
32790
±840
Bk
Undisturbed sample
32630
±730
A
Bw
13
14
15
16

Figure 4

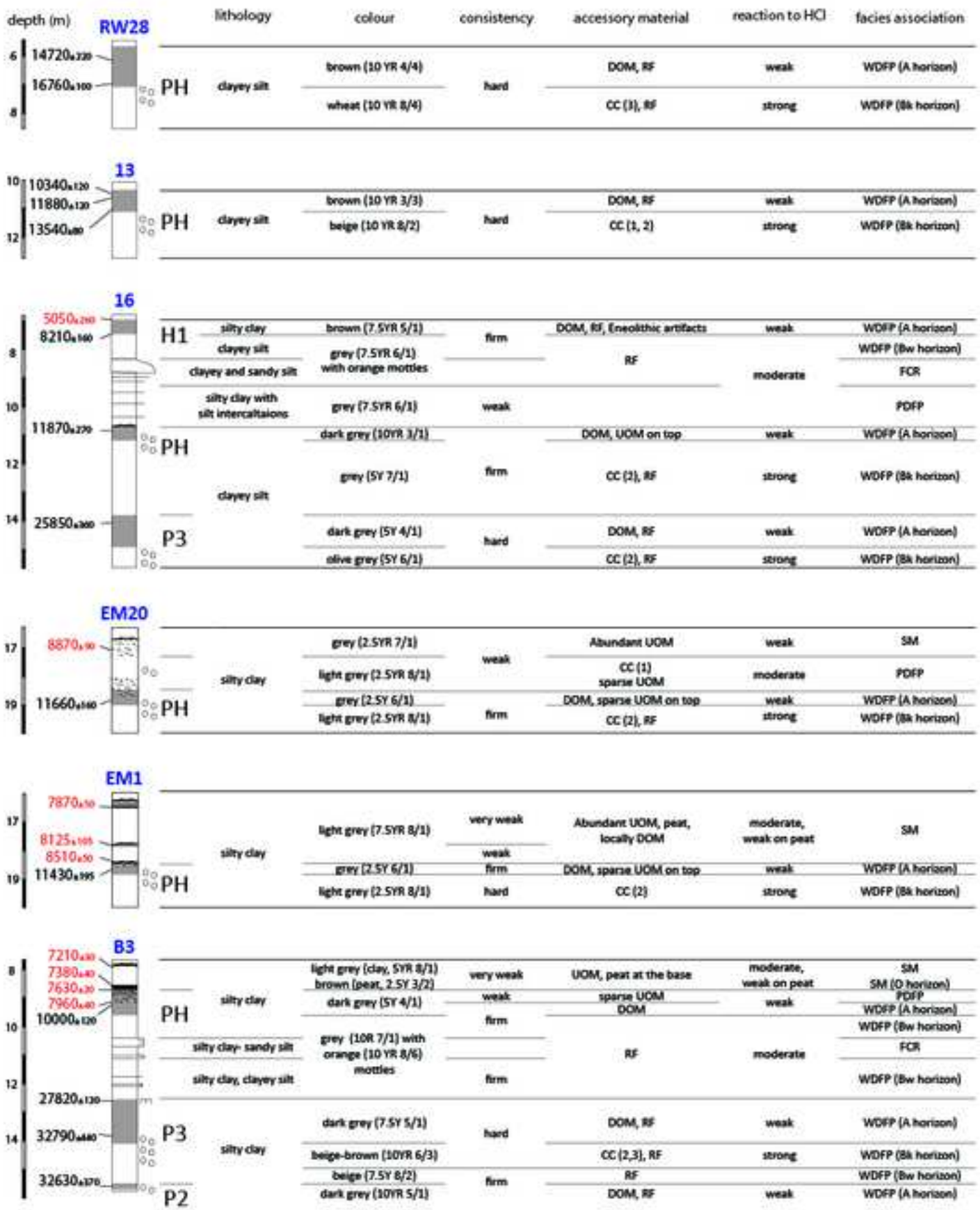
depth (m)
lithology
colour
consistency
accessory material
reaction to HCl
facies association
RW28
14720±220
16760±100
PH
clayey silt
brown (10 YR 4/4)
hard
DOM, RF
weak
WDFP (A horizon)
wheat (10 YR 8/4)
CC (3), RF
strong
WDFP (8k horizon)
13
10340±120
11880±120
13540±80
PH
clayey silt
brown (10 YR 3/3)
hard
DOM, RF
weak
WDFP (A horizon)
beige (10 YR 8/2)
CC (1, 2)
strong
WDFP (8k horizon)
16
5050±200
8210±160
11870±270
25850±300
H1
silty clay
brown (7.5YR 5/1)
firm
DOM, RF, Eneolithic artifacts
weak
WDFP (A horizon)
clayey silt
grey (7.5YR 6/1) with orange mottles
RF
moderate
WDFP (Bw horizon)
clayey and sandy silt
FCR
silty clay with silt intercaltaions
grey (7.5YR 6/1)
weak
PDFP
PH
dark grey (10YR 3/1)
DOM, UOM on top
weak
WDFP (A horizon)
clayey silt
grey (5Y 7/1)
firm
CC (2), RF
strong
WDFP (8k horizon)
P3
dark grey (5Y 4/1)
hard
DOM, RF
weak
WDFP (A horizon)
olive grey (5Y 6/1)
CC (2), RF
strong
WDFP (8k horizon)
EM20
8870±90
11660±160
silty clay
grey (2.5YR 7/1)
weak
Abundant UOM
weak
SM
light grey (2.5YR 8/1)
CC (1) sparse UOM
moderate
PDFP
PH
grey (2.5Y 6/1)
firm
DOM, sparse UOM on top
weak
WDFP (A horizon)
light grey (2.5YR 8/1)
CC (2), RF
strong
WDFP (8k horizon)
EM1
7870±50
8125±105
8510±50
11430±195
silty clay
light grey (7.5YR 8/1)
very weak
Abundant UOM, peat, locally DOM
moderate, weak on peat
SM
weak
PH
grey (2.5Y 6/1)
firm
DOM, sparse UOM on top
weak
WDFP (A horizon)
light grey (2.5YR 8/1)
hard
CC (2)
strong
WDFP (8k horizon)
B3
7210±80
7380±40
7630±20
7960±40
10000±120
27820±130
32790±480
32630±370
PH
silty clay
light grey (clay, 5YR 8/1) brown (peat, 2.5Y 3/2)
very weak
UOM, peat at the base
moderate, weak on peat
SM
SM (O horizon)
dark grey (5Y 4/1)
weak
sparse UOM
DOM
weak
PDFP
WDFP (A horizon)
firm
WDFP (Bw horizon)
silty clay- sandy silt
grey (10R 7/1) with orange (10 YR 8/6) mottles
RF
moderate
FCR
silty clay, clayey silt
firm
WDFP (Bw horizon)
P3
silty clay
dark grey (7.5Y 5/1)
hard
DOM, RF
weak
WDFP (A horizon)
beige-brown (10YR 6/3)
CC (2,3), RF
strong
WDFP (8k horizon)
P2
beige (7.5Y 8/2)
firm
RF
WDFP (Bw horizon)
dark grey (10YR 5/1)
DOM, RF
weak
WDFP (A horizon)

Figure 5

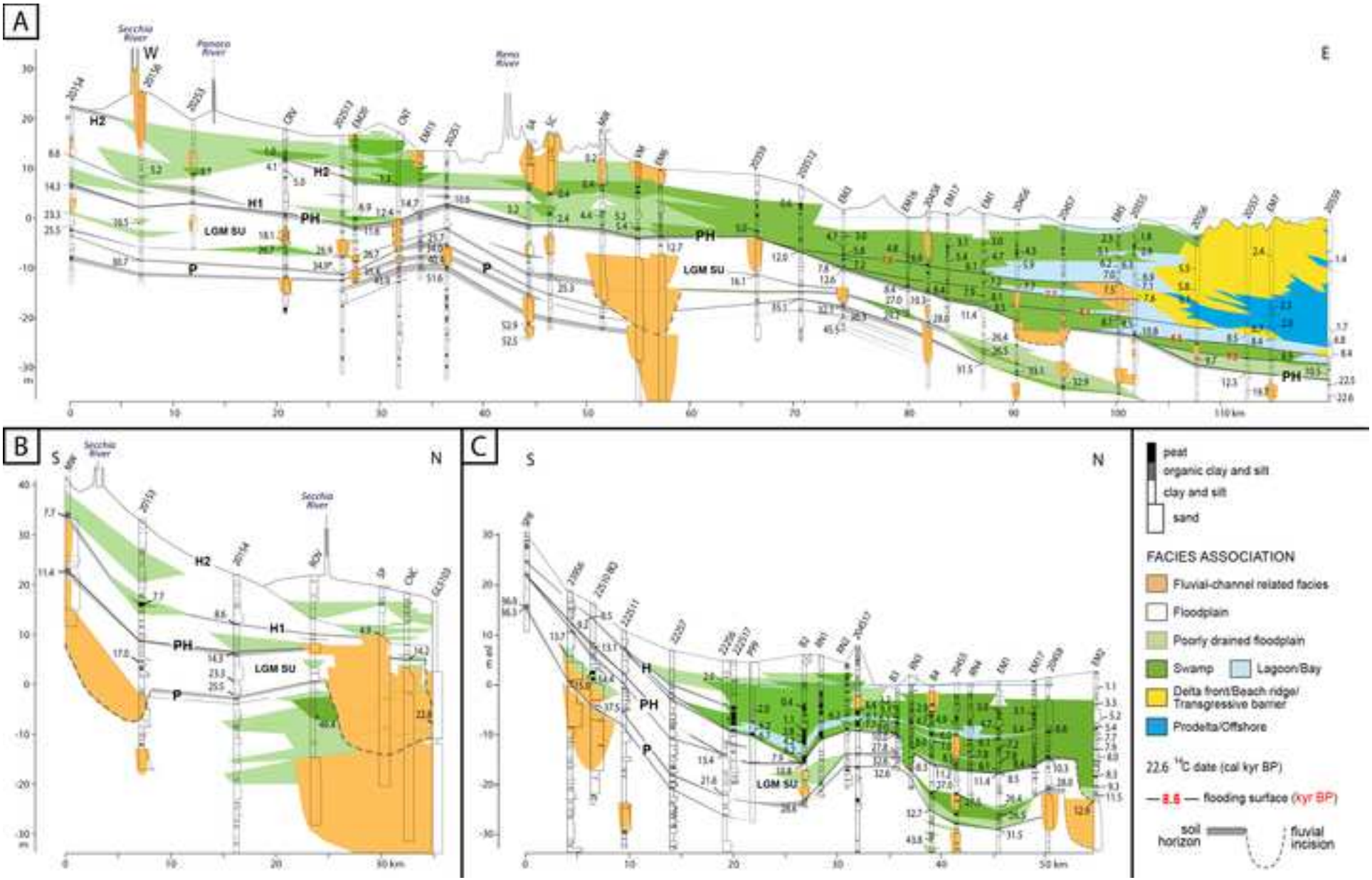
A
W
E
Secchia River
Panaro River
Reno River
H2
H1
PH
LGM SU
P
B
S
N
C
H
peat
organic clay and silt
clay and silt
sand
FACIES ASSOCIATION
Fluvial-channel related facies
Floodplain
Poorly drained floodplain
Swamp
Lagoon/Bay
Delta front/Beach ridge/ Transgressive barrier
Prodelta/Offshore
22.6 14C date (cal kyr BP)
8.6 flooding surface (kyr BP)
soil horizon
fluvial incision

Figure 6

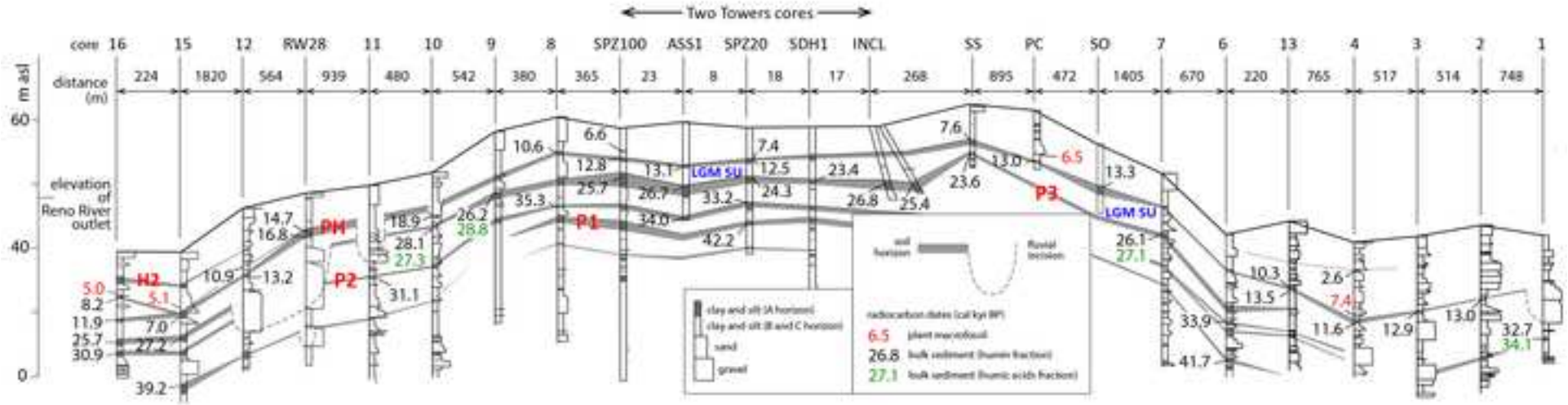
Two Towers cores
core 16 15 12 RW28 11 10 9 8 SPZ100 ASS1 SPZ220 SDH1 INCL SS PC SO 7 6 13 4 3 2 1
distance (m) 224 1820 564 939 480 542 380 365 23 8 18 17 268 895 472 1405 670 220 765 517 514 748
m asl
60
40
0
elevation of Reno River outlet
H2
P2
PH
P1
P3
LGM SU
LGM SU
5.0
8.2
11.9
25.7
30.9
5.1
7.0
27.2
39.2
10.9
13.2
14.7
16.8
18.9
28.1
27.3
31.1
26.2
28.8
35.3
10.6
6.6
12.8
25.7
13.1
26.7
34.0
42.2
7.4
12.5
33.2
24.3
23.4
26.8
25.4
7.6
23.6
13.0
6.5
13.3
26.1
27.1
10.3
13.5
33.9
41.7
2.6
7.4
11.6
12.9
13.0
32.7
34.1
clay and silt (A horizon)
clay and silt (B and C horizon)
sand
gravel
soil horizon
fluvial incision
radiocarbon dates (cal kyr BP)
6.5 plant macrofossil
26.8 bulk sediment (humin fraction)
27.1 bulk sediment (humic acids fraction)

Figure 7

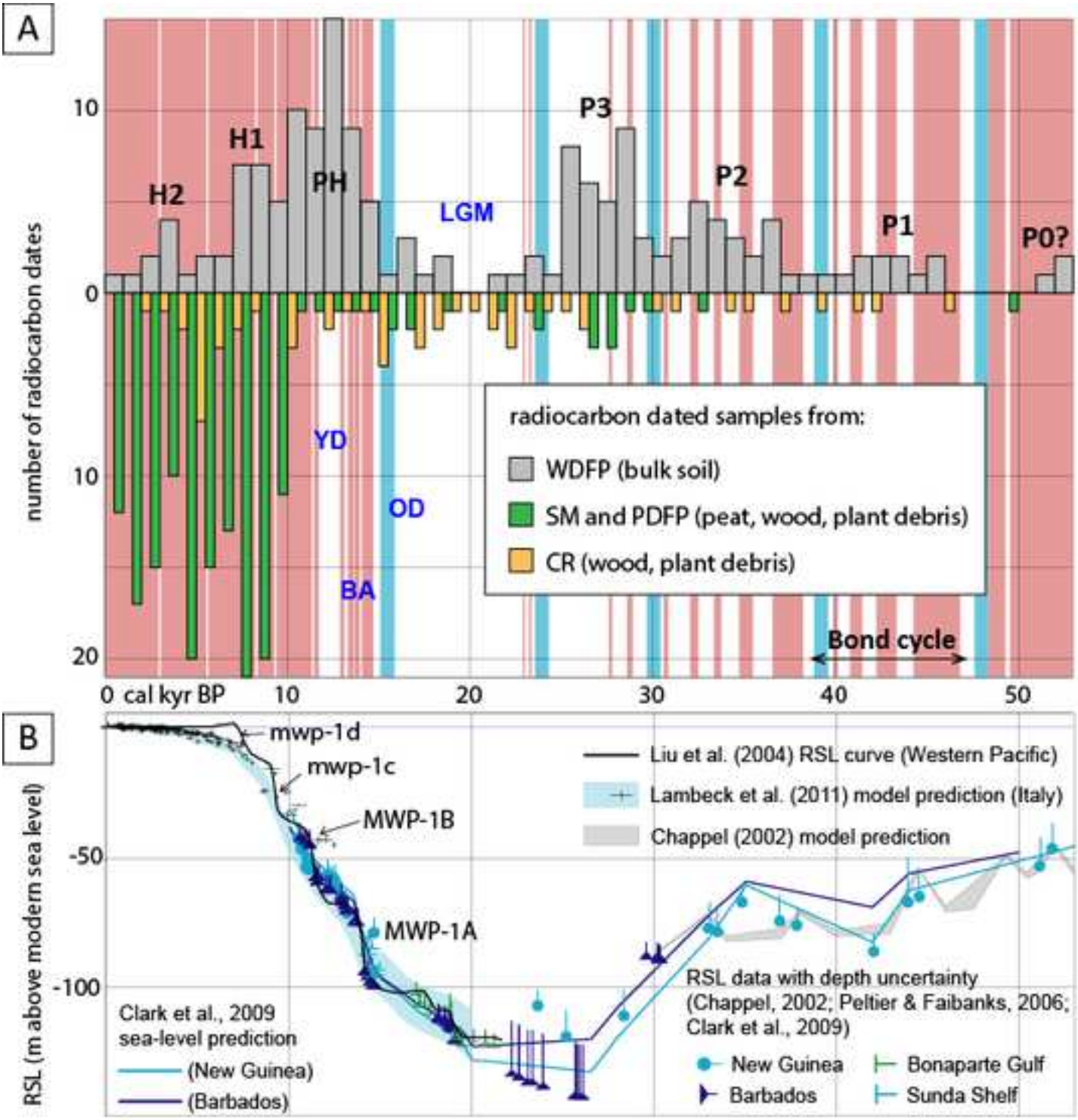
A
number of radiocarbon dates
10
0
10
20
H2
H1
PH
LGM
P3
P2
P1
P0?
YD
OD
BA
Bond cycle
radiocarbon dated samples from:
WDFP (bulk soil)
SM and PDFP (peat, wood, plant debris)
CR (wood, plant debris)
0 cal kyr BP
10
20
30
40
50
B
RSL (m above modern sea level)
-50
-100
mwp-1d
mwp-1c
MWP-1B
MWP-1A
Liu et al. (2004) RSL curve (Western Pacific)
Lambeck et al. (2011) model prediction (Italy)
Chappel (2002) model prediction
Clark et al., 2009
sea-level prediction
(New Guinea)
(Barbados)
RSL data with depth uncertainty
(Chappel, 2002; Peltier & Faibanks, 2006;
Clark et al., 2009)
New Guinea
Barbados
Bonaparte Gulf
Sunda Shelf

Figure 8

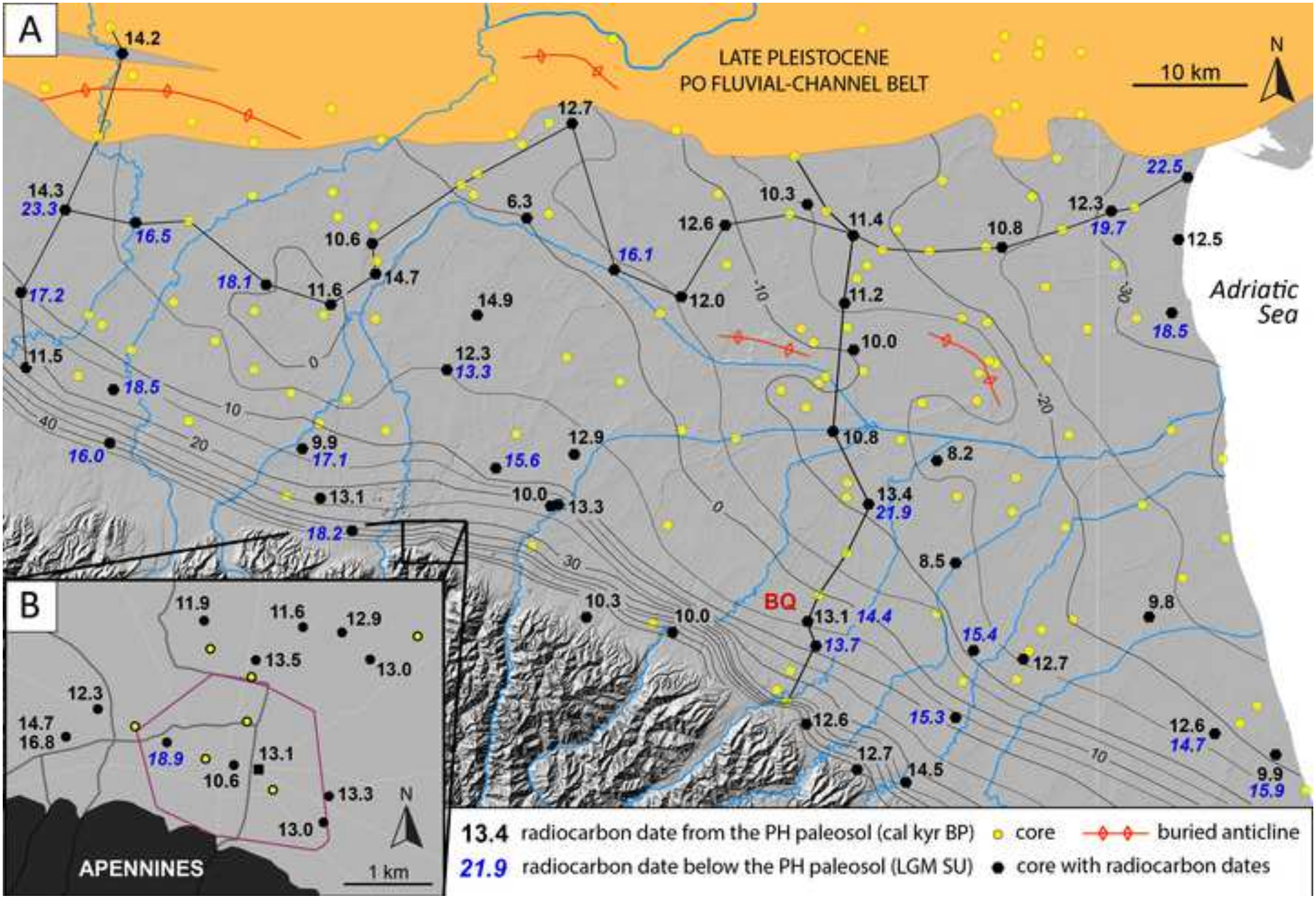
A
LATE PLEISTOCENE
PO FLUVIAL-CHANNEL BELT
10 km
N
Adriatic Sea
BQ
B
APENNINES
1 km
13.4 radiocarbon date from the PH paleosol (cal kyr BP)
21.9 radiocarbon date below the PH paleosol (LGM SU)
core
core with radiocarbon dates
buried anticline

Figure 9

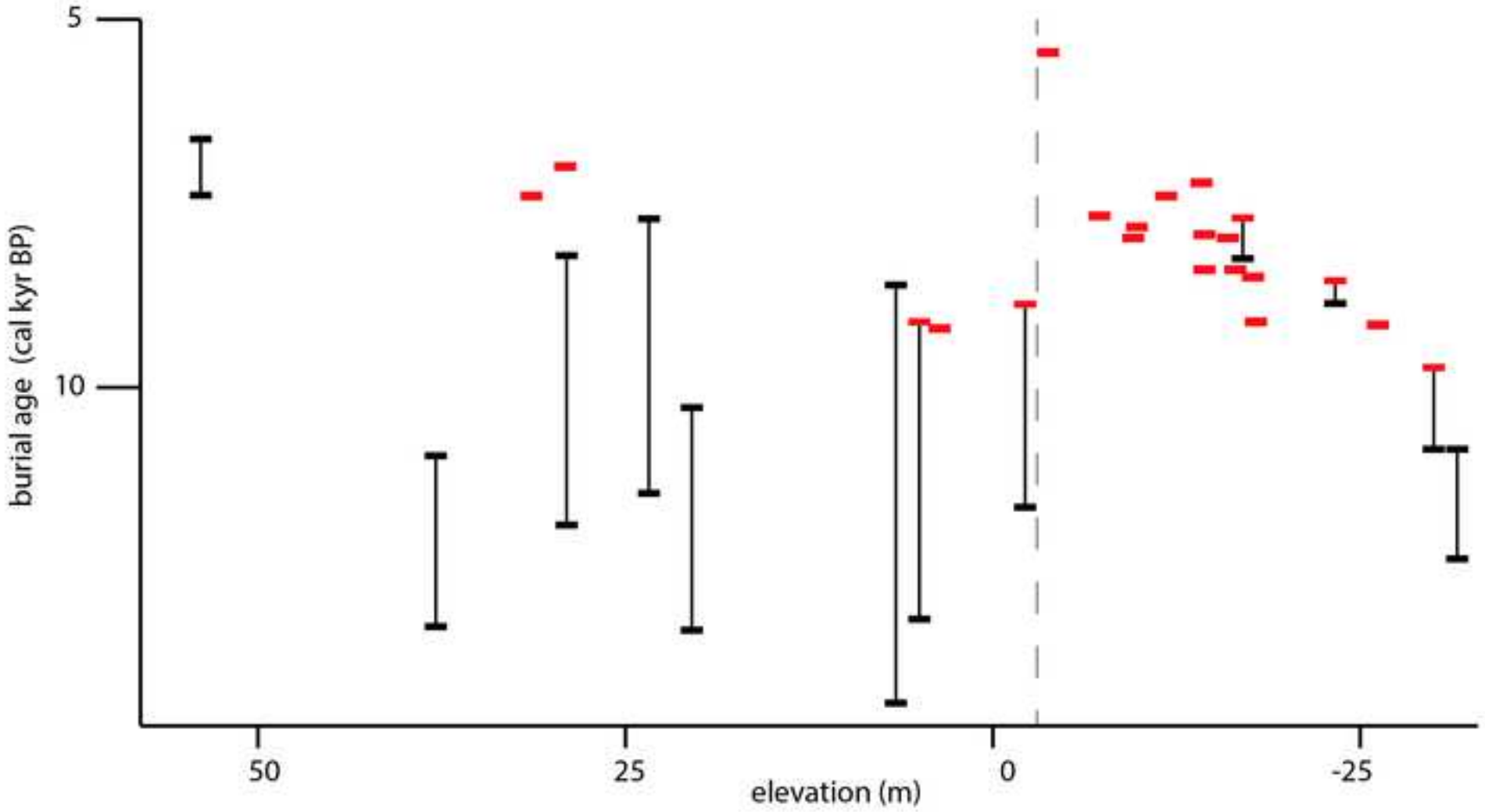

Figure 10

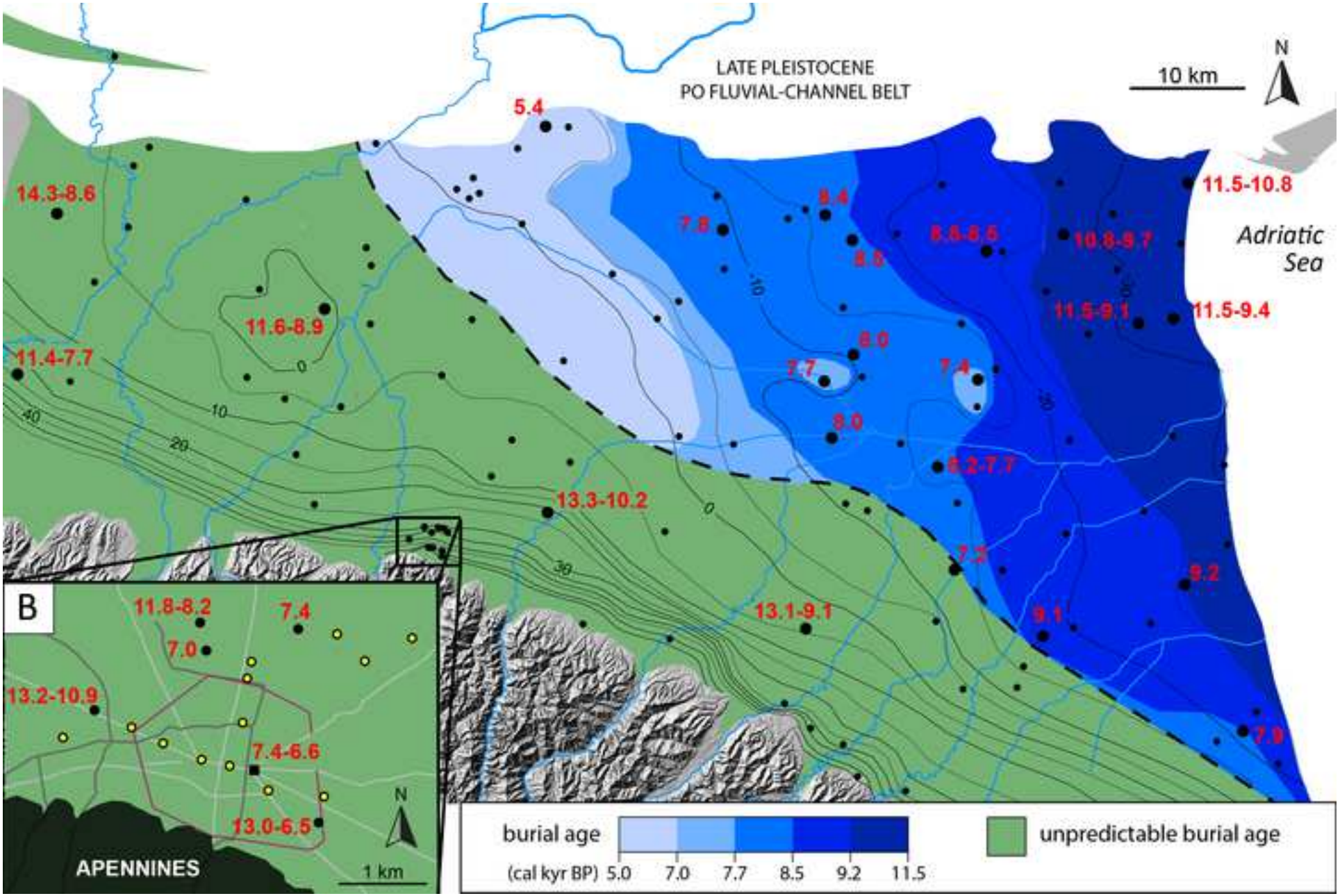
LATE PLEISTOCENE
PO FLUVIAL-CHANNEL BELT
10 km
N
Adriatic Sea
5.4
14.3-8.6
11.6-8.9
11.4-7.7
13.3-10.2
13.1-9.1
8.4
7.8
8.5
8.5-8.5
10.8-9.7
11.5-10.8
11.5-9.1
11.5-9.4
8.0
7.7
7.4
8.0
8.2-7.7
7.2
9.2
9.1
7.9
B
11.8-8.2
7.4
7.0
13.2-10.9
7.4-6.6
13.0-6.5
APENNINES
1 km
burial age
(cal kyr BP) 5.0 7.0 7.7 8.5 9.2 11.5
unpredictable burial age

**Declaration of interests**

☒ The authors declare that they have no known competing financial interests or personal relationships that could have appeared to influence the work reported in this paper.

☐The authors declare the following financial interests/personal relationships which may be considered as potential competing interests: